Light-powered CO 2 fixation in a chloroplast mimic with natural and synthetic parts

Tarryn Miller, Thomas Beneyton, Thomas Schwander, Christoph Diehl, Mathias Girault, Richard Mclean, Tanguy Chotel, Peter Claus, Niña Socorro Cortina, Jean-Christophe Baret, et al.

Light-powered CO_2 fixation in a chloroplast mimic with natural and synthetic parts

Tarryn E. Miller[1], Thomas Beneyton[3], Thomas Schwander[1], Christoph Diehl[1], Mathias Girault[3], Richard McLean[1], Tanguy Chotel[3], Peter Claus[1], Niña Socorro Cortina[1], Jean-Christophe Baret[3,4*], Tobias J. Erb[1,2*]

[1]Max Planck Institute for terrestrial Microbiology, Department of Biochemistry and Synthetic Metabolism
[2]Center for Synthetic Microbiology, Karl-von-Frisch-Str. 10, D-35043 Marburg, Germany.
[3]Univ. Bordeaux, CNRS, CRPP UMR 5031, Pessac, France.
[4]Institut Universitaire de France, Paris, France

*Corresponding author.

Email:

toerb@mpi-marburg.mpg.de (T.J.E.)

jean-christophe.baret@u-bordeaux.fr (J.-C.B.)

This document is the last submitted version of the manuscript published as

Light-powered CO_2 fixation in a chloroplast mimic with natural and synthetic parts

Science 08 May 2020, Vol. 368, Issue 6491, pp. 649-654

DOI: 10.1126/science.aaz6802

for publication on institutional repository

Abstract

Nature integrates complex biosynthetic and energy converting tasks within compartments such as chloroplasts or mitochondria. Chloroplasts convert light into chemical energy, driving CO_2 fixation. We used microfluidics to develop a chloroplast-mimic by encapsulating and operating photosynthetic membranes in cell-sized droplets. These droplets can be energized by light to power enzymes or enzyme cascades and analyzed for their catalytic properties in multiplex and real-time. We demonstrate how the micro-droplets can be programmed and controlled by adjusting internal compositions as well as using light as an external trigger. We showcase the capability of our platform by integrating the CETCH cycle, a synthetic network for CO_2 conversion, to create an artificial photosynthetic system that interfaces the natural and the synthetic biological world.

Main

The photosynthetic transformation of inorganic carbon into organic matter is a fundamental biological process, responsible for the vast majority of stored energy and biomass on Earth. This process is spatially and temporally controlled and highly integrated with other cellular functions. Photosynthesis ultimately converts light energy through membrane bound protein complexes into the energy-rich chemical cofactors adenosine triphosphate (ATP) and reduced nicotinamide adenine dinucleotide phosphate (NADPH). ATP and NADPH are subsequently used to fuel metabolic processes, in particular the fixation of carbon dioxide (CO_2) through the Calvin-Benson-Bassham (CBB) cycle (*1*).

The principle of photosynthesis has been the inspiration for artificial systems that use the energy of light for the controlled capture and conversion of CO_2 into useful compounds (*2-9*). Two recent developments in bio- and nanotechnology promise to afford integrated systems of higher efficiency, approaching or rivaling that of natural biological systems. One is the emergence of microfluidics as technology platform to manipulate and assemble constitutive elements and functions of living systems in miniaturized and confined environments (*4, 10-16*). The second is the successful design and realization of complex biomimetic modules and systems from defined biological parts. Recent examples are metabolically active micro-compartments, artificial light-harvesting organelles (*17-20*), advanced transcription-translation (TX-TL) circuits (*21, 22*) or complex *in vitro* metabolic networks (*23-25*). Yet, the combination of these individual modules into more complex systems remains a challenge (*26*). Here we developed a platform for the automated assembly of picoliter-sized reaction compartments that enable the light-driven conversion of CO_2 into multi-carbon compounds (*i.e.* glycolate), mimicking the function of chloroplasts.

In photosynthesis, thylakoid membranes provide the energy for CO_2-fixation, and we desired to exploit this ability directly for biocatalytic and synthetic biological applications. To establish a module for the light-driven regeneration of ATP and NADPH, we isolated thylakoid membranes from the chloroplasts of *Spinacia olecaera*. At 100 µmol photons m^{-2} s^{-1} these thylakoid preparations catalyzed the light-dependent reduction of $NADP^+$ to NADPH (with concomitant

oxygen evolution) at a specific activity of 3.41 ± 0.01 µmol min^{-1} $µg^{-1}$ total chlorophyll (chlorophyll A and B, referred to as Chl; **Fig. 1A**), which is comparable to values measured by others (**Table S1**). NADPH regeneration required the addition of external ferredoxin, with an optimum concentration of 5 µM. Supply of external ferredoxin:$NADP^+$ reductase (FNR) did not increase activity further (**Fig. S1A and S6A**). Addition of superoxide dismutase and catalase to scavenge reactive oxygen species (ROS) resulted in prolonged thylakoid membrane activity (**Fig. S2D**). In the following, we used light intensities between 50-60 µmol photons m^{-2} s^{-1} to further minimize the formation of ROS damaging the photosynthetic apparatus (e.g. the D1-subunit), while providing sufficient rates of NADPH regeneration (**Fig. S2E**).

Thylakoid membranes also catalyzed the regeneration of ATP from ADP, both in the light and the dark. ATP regeneration in the dark was quantified at 1.2 ± 0.2 µM min^{-1} $µg^{-1}$ Chl, attributed to membrane bound adenylate kinases (*27*), which could be suppressed by using an adenylate kinase specific inhibitor, diadenosine pentaphosphate (DAPP) (*28, 29*) (**Fig. S1C**). In the light, ATP production from ADP increased 6-fold (6.5 ± 0.5 µM min^{-1} $µg^{-1}$ Chl) and with the addition of DAPP, resulting in a light- (and ATPase-) dependent ATP synthesis rate of 5.4 ± 0.5 µM min^{-1} $µg^{-1}$ Chl (**Fig. 1B**), comparable to previous studies (**Table S1**). The specific activities of thylakoid membranes varied slightly between individual preparations (**Fig. S1E**). Thylakoid membranes were stably maintained in the dark for at least two hours at room temperature and at least 24 hours when maintained on ice with no observable loss of NADPH productivity upon illumination (**Fig. S1D**). Membrane preparations could be stored at -80 °C for more than a year without notable loss of activity (**Fig. S1E**), demonstrating their usability as thylakoid membrane-based energy modules (TEM).

Next, we tested the ability of the TEM to energize individual enzyme reactions. We coupled the TEM with two different CO_2-fixing enzymes, namely crotonyl-CoA carboxylase/reductase (Ccr) and propionyl-CoA carboxylase (Pcc), which require NADPH and ATP, respectively (**Fig. 1C**). In case of Ccr, product formation was strictly light-dependent with a CO_2-fixation rate of 5.2 ± 0.2 µM min^{-1} $µg^{-1}$ Chl (**Fig. 1D**). Pcc showed a light-dependent CO_2-fixation rate of 5.1 ± 0.2 µM min^{-1} $µg^{-1}$ Chl (**Fig. 1D**), and a low, light-independent carboxylation rate of 0.8± 0.1 µM min^{-1} $µg^{-1}$ Chl, due to the adenylate kinase activity of the TEM (see above). Notably, these carboxylation rates are more than three orders of magnitude higher than recent efforts to couple enzymatic CO_2-

fixation to isolated PSII (approx. $6.9 \cdot 10^4$ molecules h^{-1} per PSII reaction center compared to 34 molecules h^{-1} per PSII reaction center, **Table S2**), highlighting the capability of our TEM to energize catalytic transformations.

We sought to test the capacity of the TEM to not only power individual CO_2-fixing reactions, but a complete metabolic cycle for the continuous fixation of CO_2. To that end we combined the 16 enzymes of the CETCH cycle (version 5.4) (*23*), an artificial pathway for the fixation of CO_2 in vitro, and a glyoxylate/hydroxypyruvate reductase from *Escherichia coli* (Ghr) with the TEM (**Fig. 2A**). Initial efforts to operate the CETCH cycle together with the TEM failed, indicating a negative interaction of system components (**Fig. S3**). One problem was an intrinsic hydratase activity of TEMs converting crotonyl-CoA into 3-hydroxybutyryl-CoA (**Fig. S5**), which we addressed by the addition of a crotonase from *P. aeruginosa* (PhaJ) (*30*) for metabolite proof-reading (*31*). Further analysis suggested that the flavin adenine dinucleotide (FAD)-dependent enzymes methylsuccinyl-CoA oxidase (Mco) and propionyl-CoA oxidase (Pco) interfered with TEM productivity, likely due to the formation of ROS and free FAD in the enzyme preparation (**Fig. S6**). The latter is capable of directly oxidizing NADPH through the interaction with FNR (see also **Fig. S3A, S3B, S6B, S6C**). When we replaced Pco with Pcc and added Ghr as an output module (creating CETCH cycle version 6.0, **Fig. 2A**, **B, C**), the coupled system produced 156 µM glycolate from 120 µM acceptor molecule (**Fig. 2D**). Replacing Mco with a methylsuccinyl-CoA dehydrogenase (Mcd), its cognate electron transfer protein (Etf), as well as an Etf-ubiquinone oxidoreductase (creating CETCH cycle version 7.0) further improved glycolate formation from CO_2 and light (**Fig. S7**).

Above results demonstrated that the synthetic CETCH cycle can be functionally coupled to the native energy machinery of photosynthesis in a fully integrated fashion using light energy to form multi-carbon compounds from CO_2. Realizing the limitations of individual bulk experiments (e.g., sample volume, self-shading effects, number of parallel assays, and no real-time monitoring), we further envisioned to miniaturize our experimental set-up for parallelization, multiplexing and high-throughput analysis. We therefore developed a droplet-based microfluidic platform for the automated assembly of metabolically active micro-compartments that can be controlled and powered by external illumination and analyzed in real-time (**Fig. S8**).

In a first step, we encapsulated the TEM into water-in-oil (w/o) micro-droplets (300 pL; 92 µm diameter, **Fig. 3A & B**) and studied their metabolic activity by assessing NADPH fluorescence in

single droplets using microscopy (**Fig. S8 and S9**). Encapsulating thylakoid membranes produced droplets with a specifically defined number of TEM granules (~100) with a maximum droplet-to-droplet variation of 20%, which is expected from a random encapsulation process (**Fig. S10B**). We further used orthogonal fluorescent barcoding to multiplex different populations of droplets (*10*), which allowed us to quantify the local chemical and metabolic states of hundreds of individual droplets of different composition in one experiment in parallel.

We then used multiplexing to study and optimize activity of droplet-encapsulated TEM granules. $NADP^+$ photoreduction in droplets was strictly dependent on illumination and directly correlated to the number of TEM granules, following a correlation with chlorophyll content (**Fig. 3C & Fig. S11**). We observed a maximum photoreduction rate of 2.0 ± 0.1 (95% confidence interval) NADPH µmol min^{-1} $µg^{-1}$ Chl at 50 µmol photons m^{-2} s^{-1}, which is comparable to rates obtained earlier in bulk experiments. Droplet-to-droplet variation in NADPH production was largely determined by statistical fluctuations of the number of encapsulated TEM granules (**Fig. S10C**). We further characterized and optimized the operating conditions of the TEM in micro-droplets. Sorbitol at 700 mM increased stability of the TEM by several hours (**Fig. S11**). $NADP^+$ photoreduction. increased with higher light intensities from 50 to 200 µmol photons m^{-2} s^{-1}, above which NADPH production rates decreased again, likely due to photodamage of the TEM (**Fig. S12**). $NADP^+$ photoreduction was operable and stable over light-dark cycles (**Fig. S13, S14D, S15B**), demonstrating that the TEM could be switched on and off in individual droplets.

We next tested the capability of TEM-containing droplets to power individual enzyme reactions by co-encapsulation of enzymes and substrates. First, we tested Ghr that catalyzes the NADPH-dependent reduction of glyoxylate to glycolate (**Fig. 3D**). At 120 µg Chl mL^{-1} reaction mixture, 8.2 µg mL^{-1} Ghr and 50 µmol photons m^{-2} s^{-1}, we observed production of 4.7 mM glycolate (starting from 5 mM glyoxylate and only 0.8 mM $NADP^+$) after 75 minutes in the light and no production in the dark control. Varying the number of TEM granules, substrate and Ghr concentrations in individual droplet populations resulted in distinct dynamic NADPH equilibrium states (**Fig. 3D-F** and **Fig. S14**), reflecting the real-time cofactor production and consumption rates in the different populations of droplets. Light-dark cycles could be used to temporally regulate cofactor regeneration and enzyme kinetics in droplet populations (**Fig. 3F**).

The homogenous behavior of droplet populations enabled us to subsequently program the metabolic activity of reaction compartments in a predictable fashion. To demonstrate this, we created a patterned emulsion of two populations of droplets differing in TEM as well Ghr concentration. This binary emulsion was activated by illumination, resulting in distinct NADPH production rates, depending on the TEM concentration in the two droplet populations. In a subsequent dark phase, NADPH was consumed at distinct rates that were correlated to different Ghr loading of the two populations (**Fig. 3G & movie S3**), demonstrating the high level of spatial, temporal, and synchronized control over individual reaction compartments that can be achieved with our platform. Similar results were also obtained for other droplet-encapsulated enzymes that required ATP- and/or NADPH, namely propionyl-CoA synthase (Pcs) and Ccr (**Fig. S15 and** S**16**). With Ccr we measured single-enzyme CO_2-fixation rates of 6.4 µmol min^{-1} mg^{-1} Chl in droplets. Without any further optimization, these rates are more than two orders of magnitude higher than recent reports of coupling photosystem II (PSII) reaction centers to pyruvate carboxylase (*18*), comparable to values reached for PSII-coupled photoelectrochemical hydrogen production (notably without CO_2 fixation, (*5*)) and reaching levels measured for isolated chloroplasts (**Table S2**).

Having created photosynthetic micro-compartments powering single enzyme reactions, we ultimately aimed at encapsulating and screening different variants of the CETCH cycle inside TEM-containing droplets (**Fig. 4**). After further optimizing the preparation of droplets for enzymes and metabolites of the CETCH cycle (**Fig. S17**), we encapsulated different CETCH cycle versions together with TEM and monitored the dynamic equilibrium of NADPH. This allowed us to directly quantify the behavior of different CETCH variants in hundreds of micro-compartments side-by-side and in real time, which would not have been possible in bulk experiments (**Fig. 4B, 4C, & Fig. S18A-B**). Droplets with CETCH based on Mcd (version 7.0) maintained TEM activity longer than droplets containing CETCH based on Mco (version 6.0) (**Fig. S18**). Supply of an additional ATP regeneration module (Ppk and polyphosphate) did not increase activity further (**Fig. 4B & C**), suggesting that cofactor regeneration was not limiting productivity of our integrated photosynthetic system, but rather the concentration, and/or interplay of the individual components of our system, such as the stability of CoA-thioester intermediates (**Fig. S17**). Without further optimization, our integrated system was able to produce 47 ± 5 µM glycolate from CO_2 over 90

minutes in droplets (**Fig. 4D**). Thus, while overall productivity of our complex system was lowered compared to Ccr alone, it still outperforms other efforts using only single enzymes (*18*). For the full CETCH cycle, we calculated a carbon conversion efficiency of about 3.5% in our micro-compartments (NADPH consumption rate of CO_2 reduction divided by the measured maximum rate of $NADP^+$ photoreduction achieved in droplets). Overall our results demonstrated that it is possible to interface natural and synthetic biological modules in thousands of cell-sized compartments to create new-to-nature photosynthetic entities that have the potential to outcompete natural photosynthesis (i.e. because of a more efficient CO_2-fixation metabolism that does not suffer from photorespiration).

The technical capability to reconstruct, control, and study complex reaction networks in a cell-like environment will be of use for both top-down and bottom-up synthetic biology. Prototyping complex metabolic reaction cascades in miniaturized compartments has the potential to provide new means for metabolic engineering. Technical advancements, especially the development of combinatorial screening methods (*32*) and bar-coding techniques to encode reaction conditions in microfluidics-based high-throughput screening (*33*) could further enhance multiplexing capabilities and guide future efforts of testing and optimizing the CETCH cycle and other new-to-nature pathways prior to their transplantation into living cells.

Our efforts also demonstrate how natural and synthetic biological modules can be mixed and matched us to create highly integrated systems that show life-like functions. Our 'synthetic chloroplast' possesses the essential characteristics of photosynthesis that allow the formation of biological building blocks from inorganic carbon, providing the basis to develop a self-sustained, completely synthetic 'designer' carbon metabolism in our artificial organelle. Future implementation of other life characteristics, such as self-repair, reproduction, as well as information processing and regulatory circuits will further contribute to the realization of synthetic organelles and cells from the bottom-up that approach or even exceed a grade of organization, integration and functional efficiency compared to their natural counterparts (*4*).

Acknowledgements

We thank J. Zarzycki, D. Strand, and S. Burgener for enlightening discussions, and G. Stoffel for providing CoA esters. **Funding:** This work was supported by the Max Planck Society (MaxSynBio), the European Research Council grant (ERC 637675 'SYBORG'), as well as the US Department of Energy Joint Genome Institute, a DOE Office of Science User Facility (contract no. DE-AC02-05CH11231) with T.J.E. as grantee. J.-C.B. acknowledges the financial support by the 'Région Aquitaine' and by the French Government 'Investments for the Future' Programme, University of Bordeaux Initiative of Excellence (IDEX Bordeaux; (ANR)-10-IDEX-03-02). T.E.M. and R.M. were supported by the International Max-Planck Research School for Environmental, Cellular and Molecular Microbiology, Marburg, Germany. **Author contributions:** T.E.M., T.B., T.S., J.-C.B and T.J.E. conceived the project. Characterization and optimization of thylakoid preparations was done by T.E.M. Couplings of the CETCH cycle to thylakoids in bulk were performed by T.E.M. together with T.S. and C.D. The ETF:QO system as electron acceptor for Etf was developed by T.E.M and R.M. Mass spectrometric analyses were performed by N.C.S. and P.C. and the data was analyzed by T.E.M. The microfluidic platform to encapsulate thylakoids was developed by T.B. and J.-C.B. T.B. and T.E.M. planned, performed and analyzed microfluidic experiments with assistance from T.C. The software for light/dark cycles time lapse fluorescence microscopy, as well as the image processing software to analyze TEM activity in droplets was developed by M.G. Experimental data was analyzed by T.E.M., T.B., and T.J.E. The manuscript was written by T.E.M., T.B., J.-C.B. and T.J.E. with contributions from all other authors. **Competing interests:** J.-C.B. is a founder and scientific advisor at Emulseo. The authors declare no other competing interests. **Data and materials availability:** All data is available in the main text or supplemental material. The LabVIEW code used for image analysis has been deposited to GitHub (34).

References and notes

1. J. A. Bassham, A. A. Benson, M. Calvin, The path of carbon in photosynthesis. *J. Biol. Chem.* **185**, 781-787 (1950).
2. C. Liu, B. C. Colon, M. Ziesack, P. A. Silver, D. G. Nocera, Water splitting-biosynthetic system with CO_2 reduction efficiencies exceeding photosynthesis. *Science* **352**, 1210-1213 (2016).
3. K. Jensen, P. E. Jensen, B. L. Moller, Light-driven chemical synthesis. *Trends Plant Sci.* **17**, 60-63 (2012).
4. P. Schwille *et al.*, MaxSynBio: Avenues Towards Creating Cells from the Bottom Up. *Angew. Chem.* **57**, 13382-13392 (2018).
5. K. P. Sokol *et al.*, Bias-free photoelectrochemical water splitting with photosystem II on a dye-sensitized photoanode wired to hydrogenase. *Nat. Energy* **3**, 944-951 (2018).
6. J. L. Guo *et al.*, Light-driven fine chemical production in yeast biohybrids. *Science* **362**, 813-816 (2018).
7. K. K. Sakimoto, A. B. Wong, P. D. Yang, Self-photosensitization of nonphotosynthetic bacteria for solar-to-chemical production. *Science* **351**, 74-77 (2016).
8. W. Y. Zhang *et al.*, Selective aerobic oxidation reactions using a combination of photocatalytic water oxidation and enzymatic oxyfunctionalizations. *Nat. Catal.* **1**, 55-62 (2018).
9. Z. C. Litman, Y. J. Wang, H. M. Zhao, J. F. Hartwig, Cooperative asymmetric reactions combining photocatalysis and enzymatic catalysis. *Nature* **560**, 355-359 (2018).
10. T. Beneyton *et al.*, Out-of-equilibrium microcompartments for the bottom-up integration of metabolic functions. *Nat. Comm.* **9**, 2391 (2018).
11. M. Weiss *et al.*, Sequential bottom-up assembly of mechanically stabilized synthetic cells by microfluidics. *Nat. Mater.* **17**, 89-96 (2018).
12. S. Deshpande *et al.*, Spatiotemporal control of coacervate formation within liposomes. *Nat. Comm.* **10**, (2019).
13. K. Hasatani *et al.*, High-throughput and long-term observation of compartmentalized biochemical oscillators. *Chem. Commun.* **49**, 8090-8092 (2013).
14. A. Dupin, F. C. Simmel, Signalling and differentiation in emulsion-based multi-compartmentalized in vitro gene circuits. *Nat. Chem.* **11**, 32-39 (2019).
15. M. J. Booth, V. Restrepo Schild, S. J. Box, H. Bayley, Light-patterning of synthetic tissues with single droplet resolution. *Sci. Rep.* **7**, 9315 (2017).
16. R. Booth, Y. Qiao, M. Li, S. Mann, Spatial Positioning and Chemical Coupling in Coacervate-in-Proteinosome Protocells. *Angew. Chem.* **58**, 9120-9124 (2019).
17. S. Berhanu, T. Ueda, Y. Kuruma, Artificial photosynthetic cell producing energy for protein synthesis. *Nat. Comm.* **10**, 1325 (2019).
18. K. Y. Lee *et al.*, Photosynthetic artificial organelles sustain and control ATP-dependent reactions in a protocellular system. *Nat. Biotechnol.* **36**, 530-535 (2018).
19. X. Feng, Y. Jia, P. Cai, J. Fei, J. Li, Coassembly of Photosystem II and ATPase as Artificial Chloroplast for Light-Driven ATP Synthesis. *ACS Nano* **10**, 556-561 (2016).
20. B. C. Buddingh', J. C. M. van Hest, Artificial Cells: Synthetic Compartments with Life-like Functionality and Adaptivity. *Accounts Chem. Res.* **50**, 769-777 (2017).

21. A. M. Tayar, E. Karzbrun, V. Noireaux, R. H. Bar-Ziv, Synchrony and pattern formation of coupled genetic oscillators on a chip of artificial cells. *Proc. Natl. Acad. Sci. U.S.A.* **114**, 11609-11614 (2017).
22. M. Yelleswarapu *et al.*, Sigma Factor-Mediated Tuning of Bacterial Cell-Free Synthetic Genetic Oscillators. *ACS Synth. Biol.* **7**, 2879-2887 (2018).
23. T. Schwander, L. Schada von Borzyskowski, S. Burgener, N. S. Cortina, T. J. Erb, A synthetic pathway for the fixation of carbon dioxide in vitro. *Science* **354**, 900-904 (2016).
24. N. Srinivas, J. Parkin, G. Seelig, E. Winfree, D. Soloveichik, Enzyme-free nucleic acid dynamical systems. *Science* **358**, eaal2052 (2017).
25. Q. M. Dudley, A. S. Karim, M. C. Jewett, Cell-free metabolic engineering: Biomanufacturing beyond the cell. *Biotechnol. J.* **10**, 69-82 (2015).
26. M. J. Booth, V. Restrepo Schild, F. G. Downs, H. Bayley, Functional aqueous droplet networks. *Mol. Biosyst.* **13**, 1658-1691 (2017).
27. S. Murakami, H. Strotmann, Adenylate kinase bound to the envelope membranes of spinach chloroplasts. *Arch. Biochem. Biophys.* **185**, 30-38 (1978).
28. D. D. Strand, N. Fisher, D. M. Kramer, The higher plant plastid NAD(P)H dehydrogenase-like complex (NDH) is a high efficiency proton pump that increases ATP production by cyclic electron flow. *J. Biol. Chem.* **292**, 11850-11860 (2017).
29. G. E. Lienhard, I. I. Secemski, P1,P5-Di(adenosine-5')pentaphosphate, a Potent Multisubstrate Inhibitor of Adenylate Kinase. *J. Biol. Chem.* **248**, 1121-1123 (1973).
30. T. Fukui, N. Shiomi, Y. Doi, Expression and Characterization of (*R*)-Specific Enoyl Coenzyme A Hydratase Involved in Polyhydroxyalkanoate Biosynthesis by *Aeromonas caviae*. *J. Bacteriol.* **180**, 667-673 (1998).
31. J. Sun, J. G. Jeffryes, C. S. Henry, S. D. Bruner, A. D. Hanson, Metabolite damage and repair in metabolic engineering design. *Metab. Eng.* **44**, 150-159 (2017).
32. A. Kulesa, J. Kehe, J. E. Hurtado, P. Tawde, P. C. Blainey, Combinatorial drug discovery in nanoliter droplets. *Proc. Natl. Acad. Sci. U.S.A.* **115**, 6685-6690 (2018).
33. C.-M. Svensson *et al.*, Coding of Experimental Conditions in Microfluidic Droplet Assays Using Colored Beads and Machine Learning Supported Image Analysis. *Small* **15**, 1802384 (2019).
34. Data and computational codes are available at Zenodo (doi:10.5281/zenodo.3724502)
35. D. M. Peter, B. Vögeli, N. S. Cortina, T. J. Erb, A Chemo-Enzymatic Road Map to the Synthesis of CoA Esters. *Molecules* **21**, 517-517 (2016).
36. S. Rumpel *et al.*, Enhancing hydrogen production of microalgae by redirecting electrons from photosystem I to hydrogenase. *Energ. Environ. Sci.* **7**, 3296-3301 (2014).
37. I. Bernhardsgrütter *et al.*, Awakening the Sleeping Carboxylase Function of Enzymes: Engineering the Natural CO_2-Binding Potential of Reductases. *J. Am. Chem. Soc.* **141**, 9778-9782 (2019).
38. F. Galván, J. Márquez Antonio, E. Fernández, Physicochemical Properties of Ferredoxin from Chlamydomonas reinhardii. *Z. Naturforsch. Sect. C* **40**, 373 (1985).
39. K. Tagawa, D. I. Arnon, Oxidation-reduction potentials and stoichiometry of electron transfer in ferredoxins. *BBA-Bioenergetics* **153**, 602-613 (1968).
40. M. Shin, in *Methods Enzymol.* (Academic Press, 1971), vol. 23, pp. 440-447.

41. M. Nakamura, K. Saeki, Y. Takahashi, Hyperproduction of Recombinant Ferredoxins in Escherichia coli by Coexpression of the ORF1-ORF2-iscS-iscU-iscA-hscB-hscA-fdx-ORF3 Gene Cluster1. *J. Biochem.* **126**, 10-18 (1999).
42. R. J. Usselman *et al.*, Impact of Mutations on the Midpoint Potential of the [4Fe-4S]+1,+2 Cluster and on Catalytic Activity in Electron Transfer Flavoprotein-ubiquinone Oxidoreductase (ETF-QO). *Biochemistry* **47**, 92-100 (2008).
43. D. Seigneurin-Berny, D. Salvi, J. Joyard, N. Rolland, Purification of Intact Chloroplasts from Arabidopsis and Spinach Leaves by Isopycnic Centrifugation. *Curr. Protoc. Cell Biol.* **40**, 3.30.31-33.30.14 (2008).
44. R. J. Porra, The chequered history of the development and use of simultaneous equations for the accurate determination of chlorophylls a and b. *Photosynthesis Res.* **73**, 149-156 (2002).
45. J. Han, S. Gagnon, T. Eckle, C. H. Borchers, Metabolomic analysis of key central carbon metabolism carboxylic acids as their 3-nitrophenylhydrazones by UPLC/ESI-MS. *Electrophoresis* **34**, 2891-2900 (2013).
46. T. Beneyton, F. Coldren, J.-C. Baret, A. D. Griffiths, V. Taly, CotA laccase: high-throughput manipulation and analysis of recombinant enzyme libraries expressed in E. coli using droplet-based microfluidics. *Analyst* **139**, 3314-3323 (2014).
47. P. P. Kalberer, B. B. Buchanan, D. I. Arnon, Rates of Photosynthesis by Isolated Chloroplasts. *Proc. Natl. Acad. Sci. U.S.A.* **57**, 1542-& (1967).
48. U. Heber, H. Egneus, U. Hanck, M. Jensen, S. Köster, Regulation of photosynthetic electron transport and photophosphorylation in intact chloroplasts and leaves of Spinacia oleracea L. *Planta* **143**, 41-49 (1978).
49. S. G. Reeves, D. O. Hall, The stoichiometry (ATP/2e− ratio) of non-cyclic photophosphorylation in isolated spinach chloroplasts. *BBA-Bioenergetics* **314**, 66-78 (1973).
50. M. Avron, M. Gibbs, Carbon Dioxide Fixation in the Light and in the Dark by Isolated Spinach Chloroplasts. *Plant Physiol.* **53**, 140-143 (1974).
51. U. Heber, Stoichiometry of reduction and phosphorylation during illumination of intact chloroplasts. *BBA-Bioenergetics* **305**, 140-152 (1973).
52. D. Heineke, M. Stitt, H. W. Heldt, Effects of inorganic phosphate on the light dependent thylakoid energization of intact spinach chloroplasts. *Plant Physiol.* **91**, 221-226 (1989).
53. M. Stitt, Limitation of Photosynthesis by Carbon Metabolism : I. Evidence for Excess Electron Transport Capacity in Leaves Carrying Out Photosynthesis in Saturating Light and CO_2. *Plant Physiol.* **81**, 1115-1122 (1986).
54. I. Yacoby *et al.*, Photosynthetic electron partitioning between [FeFe]-hydrogenase and ferredoxin:NADP+-oxidoreductase (FNR) enzymes in vitro. *Proc. Natl. Acad. Sci. U.S.A.* **108**, 9396-9401 (2011).
55. R. Danielsson, P.-Å. Albertsson, F. Mamedov, S. Styring, Quantification of photosystem I and II in different parts of the thylakoid membrane from spinach. *BBA-Bioenergetics* **1608**, 53-61 (2004).
56. B. Nocek *et al.*, Polyphosphate-dependent synthesis of ATP and ADP by the family-2 polyphosphate kinases in bacteria. *Proc. Natl. Acad. Sci. U.S.A.* **105**, 17730-17735 (2008).
57. M. Könneke *et al.*, Ammonia-oxidizing archaea use the most energy-efficient aerobic pathway for CO2 fixation. *Proc. Natl. Acad. Sci. U.S.A.* **111**, 8239-8244 (2014).

58. J. Zarzycki *et al.*, Mesaconyl-Coenzyme A Hydratase, a New Enzyme of Two Central Carbon Metabolic Pathways in Bacteria. *J. Bacteriol.* **190**, 1366-1374 (2008).
59. T. J. Erb, L. Frerichs-Revermann, G. Fuchs, B. E. Alber, The Apparent Malate Synthase Activity of *Rhodobacter sphaeroides* Is Due to Two Paralogous Enzymes, (3*S*)-Malyl-Coenzyme A (CoA)/β-Methylmalyl-CoA Lyase and (3*S*)- Malyl-CoA Thioesterase. *J. Bacteriol.* **192**, 1249-1258 (2010).
60. M. Kitagawa *et al.*, Complete set of ORF clones of Escherichia coli ASKA library (A Complete S et of E. coli K -12 ORF A rchive): Unique Resources for Biological Research. *DNA Research* **12**, 291-299 (2005).
61. K. Hoelsch, I. Sührer, M. Heusel, D. Weuster-Botz, Engineering of formate dehydrogenase: synergistic effect of mutations affecting cofactor specificity and chemical stability. *Appl. Microbiol. Biotechnol.* **97**, 2473-2481 (2013).
62. T. J. Erb, G. Fuchs, B. E. Alber, (2S)-Methylsuccinyl-CoA dehydrogenase closes the ethylmalonyl-CoA pathway for acetyl-CoA assimilation. *Mol. Microbiol.* **73**, 992-1008 (2009).
63. T. J. Erb, J. Rétey, G. Fuchs, B. E. Alber, Ethylmalonyl-CoA Mutase from Rhodobacter sphaeroides Defines a New Subclade of Coenzyme B12-dependent Acyl-CoA Mutases. *J. Biol. Chem.* **283**, 32283-32293 (2008).
64. R. G. Rosenthal *et al.*, Direct evidence for a covalent ene adduct intermediate in NAD(P)H-dependent enzymes. *Nat. Chem. Biol.* **10**, 50-55 (2014).

Supplementary Material

Materials and Methods
Supplementary Movies 1-4
Supplementary Figures 1-18
Supplementary Tables 1-9
References 34-64

Figure Legends

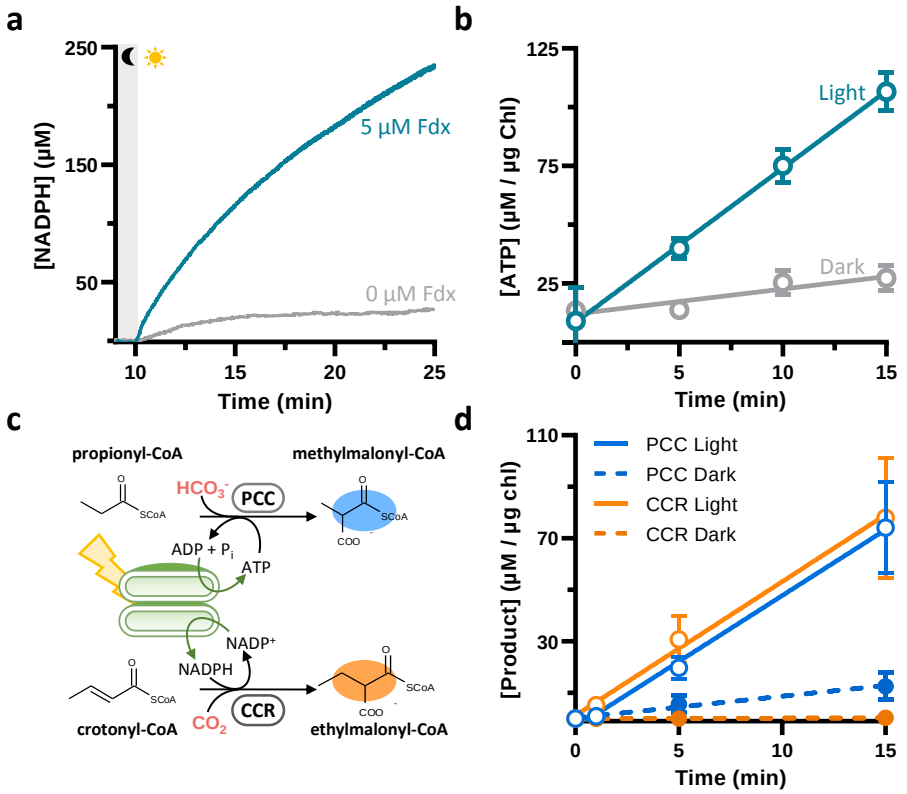

Figure 1: Light-driven cofactor regeneration by thylakoid membrane-based energy modules (TEM) (**A**) NADPH production is dependent on light and externally added ferredoxin (**B**) ATP production is dependent on light, with some background reaction in the dark due to membrane bound adenylate kinase (Fig. S1B). (**C**) Scheme of TEM-driven carboxylation reactions of propionyl-CoA carboxylase (Pcc) and crotonyl-CoA carboxylase/reductase (Ccr) utilizing light-produced ATP and NADPH, respectively. (**D**) Reactions coupled to TEM (2.5 or 5 µg Chl and 60 µmol photons m^{-2} s^{-1}) (N=6).

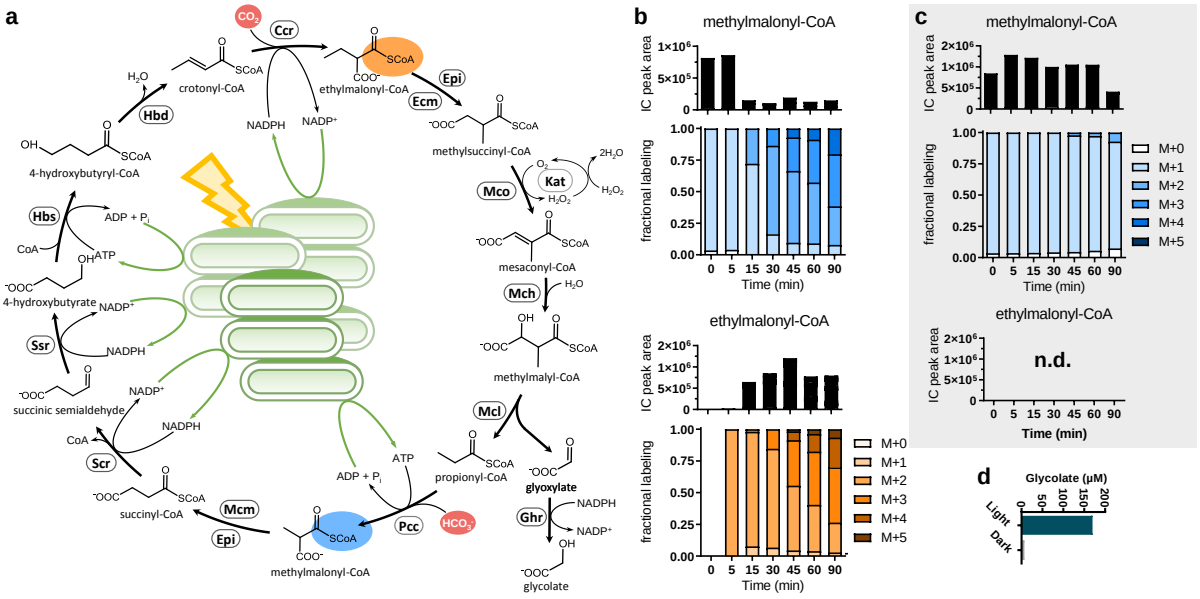

Figure 2: Light-driven, continuous fixation of CO_2 into organic acids (**A**) Scheme of CETCH version 6.0 for the conversion of CO_2 into glycolate coupled to TEM. (**B-C**) ^{13}C-labeling patterns and total levels of methylmalonyl-CoA (blue) and ethylmalonyl-CoA (orange) over time, starting the CETCH cycle with 80 µM propionyl-CoA. (**B**) CETCH cycle version 6.0 directly operated by 125 µg Chl mL^{-1} TEM under constant illumination (60 µmol photons m^{-2} s^{-1}). Shown is the extracted ion peak area and the fractional labeling of ethylmalonyl-CoA, as well as methylmalonyl-CoA (in shades of orange and blue, respectively, see Supplementary Fig. 4 for explanation of the labeling pattern) (**C**) same as in (b) but in the dark, showing that light is required to operate the cycle. Ethylmalonyl-CoA is not produced in the dark when starting from propionyl-CoA (n.d., not detected). (**D**) Glycolate production in the light and the dark by CETCH version 6.0.

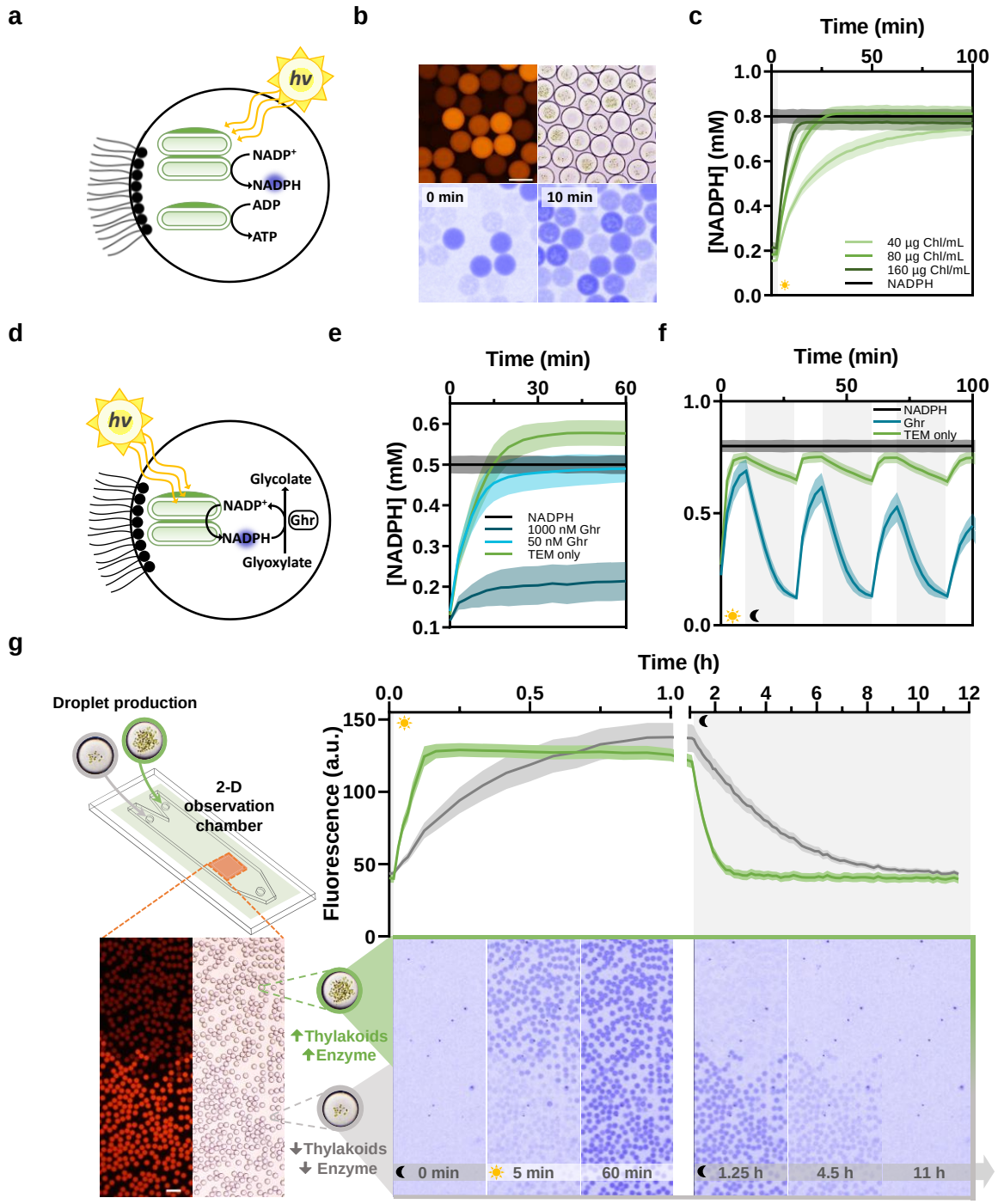

Figure 3: Encapsulation of a functional TEM in micro-droplets and light-driven enzymatic reaction coupled to TEM in micro-droplets. (**A**) Scheme of the TEM system encapsulated in micro-droplets. Light triggers TEM activity to produce NADPH and ATP. NADPH production is monitored by NADPH fluorescence (365 nm) of individual droplets. Populations of droplets can be distinguished from one another through the addition of a barcoding dye. (**B**) Microscopic pictures of a representative 4-bit emulsion of droplets containing four different TEM concentrations. First row, left to right: barcode fluorescence, bright field. Second row, left to right: NADPH fluorescence at time point 0, NADPH fluorescence after ten minutes. A time-lapse video of the increasing NADPH fluorescence is available as **movie S1**. (**c**) NADPH

concentration versus time of micro-droplets with varying TEM. (**D**) Scheme of the TEM-powered reduction of glyoxylate into glycolate by Ghr encapsulated in micro-droplets.(**E**) TEM-driven conversion (65 µg Chl mL^{-1}) of glyoxylate (5 mM) by Ghr in micro-droplets (N = 50). The concentration of Ghr changes the steady state level of NADPH at 50 µmol photons m^{-2} s^{-1} (**F**) TEM-driven conversion of glyoxylate (120 µg Chl mL^{-1} and 5 mM respectively) in micro-droplets under programmed light-dark cycles. Photoreduction of $NADP^+$ in droplets (N=50) with 53.5 nM Ghr (teal line) under alternating cycles of illumination (50 µmol photons m^{-2} s^{-1}) and darkness. Control: Droplets containing no Ghr (green line) and droplets containing 1 mM NADPH (black line). A time-lapse video of oscillations is available as **movie S2**. In c, e, and f, bold lines indicate the mean of the droplet population. Shaded areas indicate the ± standard deviation (N=50). (**G**) Time and space control of metabolic activity in droplets. A binary emulsion of droplets with two different TEM and Ghr concentrations was created. A spatial pattern was created by filling the droplets into an observation chamber, with each population filling approximately half of the chamber. The plot shows relative NADPH fluorescence over time under fluctuating light conditions (dark, 50 µmol photons m^{-2} s^{-1}, dark) for both droplet populations, with the same color coding. A time-lapse video of NADPH fluorescence is available as **movie S3**.

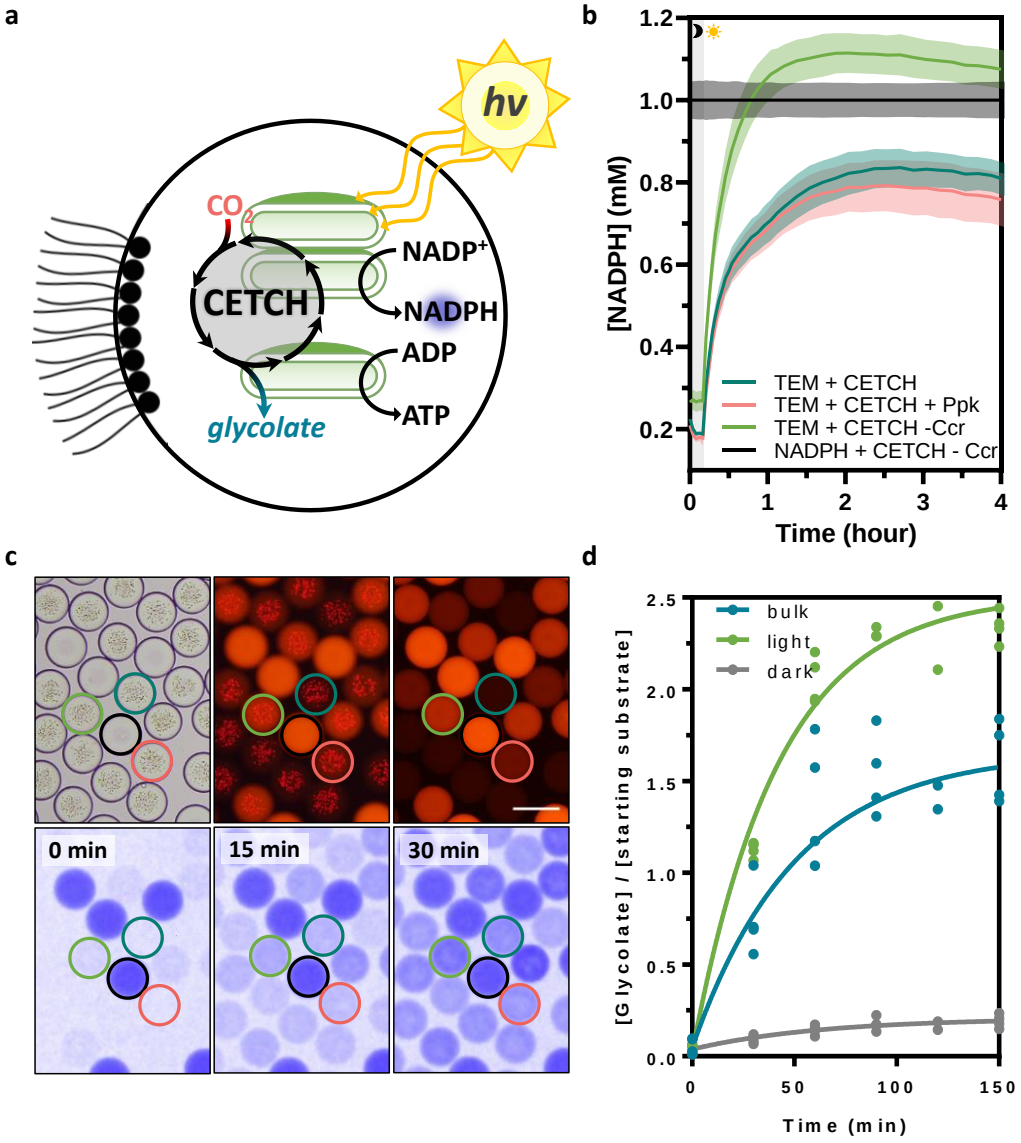

Figure 4: Light-driven, continuous fixation of CO_2 into organic acids by CETCH version 7.0 coupled to TEM in micro-droplets. (**A**) Scheme of the CETCH version 7.0 coupled to TEM operating inside micro-droplets. (**B**) Dynamic equilibrium states of NADPH fluorescence of four populations of droplets: Droplets containing TEM (60 µg Chl mL^{-1}), 1 mM $NADP^+$ and CETCH version 7.0 (teal line), droplets containing TEM, 1 mM $NADP^+$ and an additional ATP regeneration system (Ppk and polyphosphate, coral line), as well as control droplets containing 1 mM NADPH and all CETCH version 7.0 components except for Ccr (black line), and control droplets containing TEM, 1 mM $NADP^+$ and all CETCH version 7.0 components except for Ccr (green line). (**C**) Images of the droplets from (B) using the same color coding; first row, left to the right: bright field, thylakoid fluorescence with overlap from the coding dye, coding dye; second row, left to the right: NADPH fluorescence before illumination, after 15 minutes, and after 30 minutes illumination (scale bar corresponds to 100 µM). A time-lapse video is available as **movie S4**. (**D**) Glycolate formed per acceptor molecule (sum of crotonyl-CoA and 3-hydroxybutyryl-CoA) over time in droplets and in bulk solution. The light and dark curves represent droplets maintained in the light and in the dark. The

bulk curve shows an experiment with the same reaction mixture but on the micro-tube scale, kept in the dark for the duration of droplet manufacture. The bulk solution and the droplets were simultaneously exposed to light for parallel comparison.

Supplementary Materials for

Light-powered CO_2 fixation in a chloroplast mimic with natural and synthetic parts

Tarryn E. Miller, Thomas Beneyton, Thomas Schwander, Christoph Diehl, Mathias Girault, Richard McLean, Tanguy Chotel, Peter Claus, Niña Socorro Cortina, Jean-Christophe Baret*, Tobias J. Erb*

*Corresponding author. Email: toerb@mpi-marburg.mpg.de (T.J.E.), jean-christophe.baret@u-bordeaux.fr (J.-C.B.)

This PDF file includes:

Materials and Methods

Captions for Movies S1 to S4

Figs. S1 to S18

Tables S1 to S9

References

Other Supplementary Materials for this manuscript include the following:

Movies S1 to S4

Materials and Methods

Materials

Chemicals were purchased from Sigma-Aldrich (Munich, Germany) and CARL ROTH GmbH (Karlsruhe, Germany). Sulforhodamine B and 1H, 1H, 2H, 2H-perfluoro-1-octanol were purchased from Sigma. $Na^{13}CO_3H$ was obtained from Cambridge Isotope Laboratories Inc. (Tewksbury, USA) and 3-hydroxypropionate was bought from TCI Deutschland GmbH (Eschborn, Germany). Fluoro-silane (Aquapel) was purchased from Aquapel Glass Treatment (Pittsburgh Glass Works LLC Pittburgh, PA, USA). Coenzyme A was purchased from Roche Diagnostics. Biochemicals and materials for cloning and expression were obtained from Thermo Fisher Scientific (St. Leon-Rot, Germany), New England Biolabs GmbH (Frankfurt am Main, Germany), and Macherey-Nagel GmbH (Düren, Germany). Carbonic anhydrase was bought from MP Biomedicals (Illkirch, France). Primers were obtained from Eurofins MWG GmbH (Ebersberg, Germany). Synthesized genes were obtained from Eurofins MWG GmbH (Ebersberg, Germany) or BaseClear B.V. (Leiden, Netherlands). Materials and equipment for protein purification were obtained from GE Healthcare (Freiburg, Germany), Bio-Rad (Munich, Germany) or Merck Millipore GmbH (Schwalbach, Germany).

CoA-Thioester synthesis

Crotonyl-CoA and propionyl-CoA were synthesized from their respective anhydrides according to D. Peter et al. (*35*). (*S*)-methylsuccinyl-CoA and mesaconyl-CoA were synthesized via the mixed anhydride method starting from the free acids and obtaining a racemic mixture of 2-(*S*)-methyl and 3-(*S*)-methyl-thioester. Ethylmalonyl-CoA and methylmalonyl-CoA were enzymatically produced with either crotonyl-CoA carboxylase or propionyl-CoA carboxylase starting from crotonyl-CoA or propionyl-CoA according to Schwander et al. and Peter et al. (*23, 35*). All CoA-thioesters were purified using a HPLC (1260 Infinity, Agilent Technologies GmbH) with a Gemini® 10µm NX-C18 110 Å Column (Phenomenex, Aschaffenburg, Germany) as described previously (*23, 35*). The concentration of CoA-esters was quantified by determining the absorption at 260 nm ($\varepsilon = 22.4\ mM^{-1}\ cm^{-1}$ for unsaturated and $\varepsilon = 16.4\ mM^{-1}\ cm^{-1}$ for saturated CoA-thioesters).

Cloning and Mutagenesis

Chlamydomonas reinhardtii ferredoxin, spinach ferredoxins, and spinach ferredoxin:$NADP^+$ oxidoreductase (FNR) lacking the transit peptides were codon optimized for enzyme production in *E. coli* by Eurofins Genomics Germany GmbH (Ebersberg, Germany). They were cloned into pET16b, pET28b, or pASK-IBA7 with the addition of an N-terminal Strep-tag. A *C. reinhardtii* FNR expression plasmid was provided by Dr. Winkler and described in Rumpel et al. (*36*). The *Rhodobacter sphaeroides* 2.4.1 electron transport flavoprotein-ubiquinone oxidoreductase was cloned from genomic DNA (using the forward 5'-TAT ACA TAT GAC CGA GCA GAC TCC C and reverse 5'-TAT AGG TCT CGG ATC CTC ACA TGT TGG GAT AGT TCG primers) into pET16b vector containing a Strep-tag using NdeI and BamHI. The PCR product was cut with BsaI and NdeI to avoid the naturally occurring internal BamHI sites. The *Pseudomonas migulae* electron transport flavoprotein-ubiquinone oxidoreductase was codon optimized and synthesized by BaseClear B.V. (Leiden, Netherlands).

General protein production and purification

Enzymes were produced in *Escherichia coli* strains BL21(DE3), BL21(DE3) AI, Rosetta 2 (DE3) pLysS, C41(DE3) pLysS pRKisc, and BL21(DE3) ΔiscR. Cells were grown in terrific broth at 37 °C using the appropriate antibiotic for selection (100 µg/ml ampicillin, 50 µg/ml kanamycin, 34 µg/ml chloramphenicol, 20 µg/ml Streptomycin, 10 µg/ml tetracycline, and 50 µg/ml spectinomycin). Unless otherwise noted, when an OD_{600} = 0.7-1.0 was reached the culture was cooled to 23°C and induced by the addition of 500 µM IPTG (Isopropyl-D-β-thiogalactopyranoside) or 200 µg/L anhydrotetracycline. When using *E. coli* BL21(DE3) AI as an expression host 0.02 % (w/v) L-arabinose was additionally added. After 14-18 hours the cells were harvested for 12 min at 6,600 × g at 4 °C. Unless immediately purified, cell pellets were frozen and stored at -20° or -80° C. Unless otherwise specified, His-tagged enzymes were purified by resuspending the cell pellet 1:2 (w/v) ratio in Buffer L (50 mM HEPES pH 8.0 or 20 mM Tris-HCl pH 8.1, 500 mM NaCl, 5 mM $MgCl_2$, 10% glycerol, and DNAse) and lysed by ultrasonication. The lysate was clarified by ultracentrifugation (1 hour at 100,000 × g) and the resulting supernatant was filtered through a 0.45 or 0.2 µm filter. Lysate was loaded onto a HisTrap FF (GE Healthcare,

Freiburg, Germany) and unspecifically bound protein was removed with a buffer containing: 50 mM HEPES-KOH pH 8.0 or 20 mM Tris-HCl pH 8.1, 500 mM NaCl, and 75 mM imidazole. The protein was eluted in 50 mM HEPES-KOH pH 8.0 or 20 mM Tris-HCl pH 8.1, 500 mM NaCl, and 500 mM imidazole. The eluted protein was either desalted in a buffer containing: 50 mM HEPES-KOH pH 8.0 or 20 mM Tris-HCl pH 8.1, and 150 mM NaCl with a HiTrap 5 ml Desalting (GE Healthcare, Freiburg, Germany) column or by gel filtration using a HiLoad 16/600 Superdex 200 pg (GE Healthcare, Freiburg, Germany) size exclusion column equilibrated with a buffer containing: 50 mM HEPES-KOH pH 8.0 or 20 mM Tris-HCl pH 8.1, and 200 mM NaCl. Elution fractions were concentrated with Amicon Ultra-4 centrifugal filters (Merck Millipore, Darmstadt, Germany). Purified proteins were stored in 30-50% Glycerol at -20°C or -80°C and the concentration was determined on a Nanodrop 2000 (Thermo Scientific, St. Leon-Rot, Germany) from extinction coefficients calculated on ProtParam, unless otherwise specified.

Recombinant production and purification of 4-hydroxybutyryl-CoA dehydratase (Nmar0207), 4-hydroxybutyryl-CoA synthetase (Nmar0206), and 2-(*S*)-methylsuccinyl-CoA oxidase (Mco) was purified as described in Schwander et al *(23)*. However, the resulting protein solution was flash frozen and stored at -80°C. This increased the stability of some of the enzymes from days or weeks to months (*23*). Codon optimized propionyl-CoA synthase (Pcs) was produced and purified according to Bernhardsgrütter et al. (*37*).

Recombinant protein production and purification of Chlamydomonas and Spinach ferredoxins

Ferredoxins were produced in C41(DE3) pLysS pRKisc, or BL21(DE3) ΔiscR cultures were grown to an OD_{600} of 0.7-0.9 and cooled to 23 °C and induced by the addition of 500 μM IPTG and ammonium ferric citrate was added (260 mg per liter of growth media). Cells were harvested after 14-18 h as described above. Cell pellets were resuspended in a lysis buffer (50 mM HEPES-KOH pH 7.8, 150 mM NaCl, 2 mM DTT, and 10% glycerol) at 2 mL per gram of pellet. The cells were lysed and clarified as above. The supernatant was loaded onto a StrepTrap HP (GE Healthcare, Freiburg, Germany) equilibrated with the lysis buffer or a buffer without the glycerol. The unbound protein was washed with the same buffer. Elution was carried out in the same buffer with the addition of 2.5 mM desthiobiotin. The resulting protein was concentrated as described

above, but quantified using the following extinction coefficients: *Chlamydomonas* ferredoxin, 8.38 mM cm^{-1} at 420 nm (*38*); *Spinacia oleracea* ferredoxin, 9.68 mM cm^{-1} at 420 nm (*39*).

Recombinant protein production and purification of *Chlamydomonas* and Spinach Ferredoxin $NADP^+$ reductase (FNR)

Strep-tagged FNR from both *S. oleracea* and *C. reinhardtii* were produced in BL21(DE3) as described above. Cells were lysed in a buffer containing 50 mM HEPES-KOH pH 7.8, 150 mM NaCl, and 10% glycerol. Lysis and clarification were performed as above and loaded onto a StrepTrap HP (GE Healthcare, Freiburg, Germany). It was washed with a buffer containing 50mM HEPES-KOH pH 7.8 and 150 mM NaCl and eluted in a buffer containing 2.5-5 mM desthiobiotin. The protein was concentrated in an Amicon and 40% glycerol was added as a cryoprotectant prior to freezing. The concentration for both *C. reinhardtii* and Spinach FNR were determined using the extinction coefficient, 10.74 mM cm^{-1} at 456 nm (*40*).

Electron transport flavoprotein-oxidoreductase (ETF:QO) protein production and purification

ETF:QO enzymes were produced in BL21(DE3) or C41(DE3) harboring both the pLysS, and the pRKisc plasmid for iron-sulfur cluster formation (*41*). Cells were grown, induced, and harvested according to the basic protocol above. The enzyme was purified based on a modified method from Usselman et al. (*42*). Cell pellets were resuspended in 1:3 ratio (w/v) in buffer A (50 mM Tris-HCl pH 7.6, 500 mM NaCl, and 0.1 mM DTT), prior to lysis and 10 µg/mL DNAseI was added. Cells were lysed by French press or ultrasonication and the insoluble fractions were harvested by ultracentrifugation for 1 hour at 100,000 × g. The supernatant was removed and the resulting pellet was washed in buffer A and centrifuged again. A rough protein concentration of the pellet was determined with the Pierce™ Rapid Gold BCA Protein assay kit (Thermo Scientific). The pellet was resuspended in buffer A to approximately 20 mg protein/mL. The pellet was solubilized by adding dodecyl-β-D-maltoside at a ratio of 2.5:1 (w/w) of protein to dodecyl-β-D-maltoside and shaking for 90 minutes at 8°C. The solution was centrifuged for a third time for 1 hour at 100,000 × g and the resulting supernatant was diluted 10-fold in buffer A, filtered with a 0.45 µm syringe filter, and loaded onto a StrepTrap HP or HisTrap FF (rsETF:QO and

pmETF:QO, respectively). The washing and elution of the enzymes was done according to the protocols above for His and Strep-tagged proteins.

Chloroplast Isolation

Chloroplasts were isolated from young spinach purchased from the local market or grocery store using a modified method from (*28*, *43*). Spinach leaves were stored in the dark at 4-8 °C until use. The leaves were washed and the large stems were removed and buffer was added at a ratio of 1 g plant material to 1 mL cold buffer (330 mM sorbitol, 50 mM HEPES-KOH pH 7.6, 5 mM $MgCl_2$, 0.1% (w/v) bovine serum albumin) and blended using a standard kitchen immersion blender. The resulting solution was pressed through a piece of fine mesh cotton fabric and the filtrate was centrifuged for 10 min at 3000 × g. The pellet was gently resuspended in buffer (300 mM sorbitol, 50 mM HEPES-KOH pH 7.6, 5 mM $MgCl_2$, 2 mM EDTA, and 10 mM sodium L-ascorbate,), using a fine paint brush to remove any clumps. This was overlaid on an 80/40% percoll gradient (80%: 80% v/v percoll, 10 mM sodium L-ascorbate, 300 mM sucrose, 66 mM MOPS-KOH pH 7.6 and 40%: 40% v/v percoll, 10 mM sodium L-ascorbate, 300 mM sucrose, 25 mM MOPS-KOH pH 7.6). The fractions containing thylakoids and intact chloroplasts were pooled and diluted in buffer and centrifuged for 10 min at 3000 × g. The pellet was resuspended in osmotic shock buffer (10 mM HEPES-KOH, 10 mM $MgCl_2$, 10 mM sodium L-ascorbate). Thylakoids were flash frozen with 10% DMSO as an osmoprotectant and stored at -80°C until use. The thylakoid/chloroplast solutions were maintained in darkness.

Before use, thylakoids were stored on ice and washed 2-3 times in a buffer containing: 0, 330, or 700 mM sorbitol, 10 mM HEPES-KOH pH 7.6, 10 mM $MgCl_2$, and 10 mM sodium L-ascorbate. The chlorophyll content of the resulting solution was determined according to Porra 2002 (*44*).

Assays of Thylakoid activity

Spectrophotometric observation of $NADP^+$ photoreduction and the ferredoxin titration.

TEM activity was assayed by monitoring NADPH production spectrophotometrically in a 5 mm quartz cuvette at 340 nm on a UV-Vis spectrophotometer (Cary 60 UV-Vis, Agilent Technologies GmbH). In a reaction volume of 0.7 mL, TEM was added to reach a total of 10 µg of chlorophyll to a reaction buffer containing: 50 mM HEPES-KOH pH 7.8, various ferredoxin

concentrations, 3 mM ADP, 5 mM of K_2HPO_4, 3mM $NADP^+$, 10 mM sodium L-ascorbate, 10 mM KCl, 5 mM $MgCl_2$, 1.5 µM *E. coli* catalase, and 52 U mL^{-1} of bovine superoxide dismutase and illuminated with white light at 50-100 µmol photons m^{-2} s^{-1}. Initially, various ferredoxins (SpFdx1, SpFdx2, & CrFdx1) were tested with minimal differences in activity. Ultimately, for the ferredoxin titration 0, 2.5, 5, 10, 25, and 50 µM of CrFdx1 was assayed. The concentration of NADPH was calculated using an extinction coefficient of 6.22 mM cm^{-1}.

ATP/NADPH ratio

The ATP/NADPH production ratio was determined using a similar reaction mixture (0.7 mL) listed above, with the inclusion of 700 mM sorbitol. The NADPH production was monitored spectrophotometrically in a 5 mm quartz cuvette at 340 nm on a UV-Vis spectrophotometer (Cary 60 UV-Vis, Agilent Technologies GmbH) and the concentration was determined. To trigger TEM activity, a white light was used at 60 µmol photons m^{-2} s^{-1}. Samples for ATP measurements were taken at 0, 5, 15, 30 minutes after illumination and quenched with 5% formic acid. The samples were immediately measured by HPLC-MS as described below. The concentrations were calculated using a standard curve. Standard solutions were made using commercially available ATP prepared in a buffer reflective of assay conditions for accurate concentration calculation.

ATP production rate

The ATP production rate was determined in a reaction buffer (0.2 mL) containing: 50 mM HEPES-KOH pH 7.6, 10 mM sodium L-ascorbate, 700 mM sorbitol, 5 mM $MgCl_2$, 5 mM K_2HPO_4, 10 mM KCl, 5 µM of CrFdx1, 2 mM $NADP^+$, 2 mM ADP, 1.5 µM of catalase, and 52 U mL^{-1} of bovine superoxide dismutase, and if DAPP was added, it was at 20 µM. Thylakoids were added at 2.5 µg and 10 µg chlorophyll and assayed both in the dark and in the light at 60-70 µmol photons m^{-2} s^{-1}. Samples were taken at 0, 5, 10, and 15 minutes and quenched with a final concentration of formic acid of 5%. ATP was measured with HPLC-MS by the method described below. The concentrations were calculated using a standard curve. Standard solutions were made using commercially available ATP prepared in a buffer reflective of assay conditions for accurate concentration calculation.

Oxygen evolution and NADPH production

Simultaneously, the rates of O_2 evolution and NADPH production were measured in an assay volume of 0.7 mL in a reaction buffer containing: 50 mM HEPES-KOH pH 7.6, 10 mM sodium L-ascorbate, 700 mM sorbitol, 5 mM $MgCl_2$, 5 mM K_2HPO_4, 10 mM KCl, 5 µM of CrFdx1, 3 mM $NADP^+$, 2 mM ADP, 1.5 µM of catalase, 52 U mL^{-1} of bovine superoxide dismutase, and 30 µM DAPP. Thylakoids were added at a total of 10 µg chlorophyll and assayed both in the dark and in the light at 60-70 µmol photons m^{-2} s^{-1}. NADPH production was measured as discussed above. The O_2 evolution was measured with a PyroScience fiber optic oxygen probe, either an optically isolated minisensor (OXF1100-OI) or microsensor (OXF50-OI). The NADPH production was measured in a spectrophotometer in a 5mm quartz cuvette at 340 nM. A decrease of O_2 was observed in reaction mixtures that lacked thylakoids, and this was used for a baseline correction of samples.

Oxygen evolution at different light intensities or with and without catalase and SOD

The O_2 evolution was measured at different light intensities with a PyroScience fiber optic oxygen probe, either an optically isolated minisensor (OXF1100-OI) or microsensor (OXF50-OI). The rates were measured in an assay volume of 0.4 mL in a reaction buffer containing: 50 mM HEPES-KOH pH 7.6, 10 mM sodium L-ascorbate, 700 mM sorbitol, 5 mM $MgCl_2$, 5 mM K_2HPO_4, 10 mM KCl, 5 µM of CrFdx1, 3 mM $NADP^+$, 2 mM ADP, either with or without 1.5 µM of catalase, and 52 U mL^{-1} of bovine superoxide dismutase. Thylakoids were added at a total of 10 µg chlorophyll and assayed both in the dark, 30, 60, or 300 µmol photons m^{-2} s^{-1}. There was a decrease in O_2 levels in the dark and this decrease was subtracted from the samples in the light.

Oxygen evolution during Carbon fixation

The O_2 production from TEM during the fixation of carbon (by Ccr and Pcc) was measured in an assay volume of 0.5 mL. The reaction mixture was comprised of 50 mM HEPES-KOH pH 7.6, 10 mM sodium L-ascorbate, 700 mM sorbitol, 5 mM $MgCl_2$, 5 mM inorganic phosphate (K_2HPO_4), 10 mM KCl, 5 µM of CrFdx1, 0.6 mM Propionyl-CoA, 1 mM Crotonyl-CoA, 1 mM $NADP^+$, 0.5 mM ADP, 30 nM carbonic anhydrase, 1.5 µM of catalase, 52 U mL^{-1} of bovine

superoxide dismutase, 1.3 µM Ccr, and 1.8 µM Pcc, and 30 µM DAPP. Thylakoids were added at a rate of 7.5µg total chlorophyll. The reactions were assayed, both in the dark and illuminated at 60-70 µmol photons m^{-2} s^{-1}. O_2 was measured using the PyroScience fiber optic oxygen probe with either an optically isolated minisensor (OXF1100-OI) or microsensor (OXF50-OI). There was a decrease in O_2 levels in the dark and this was used as a baseline correction. To measure product formation from Pcc or Ccr, samples were taken at 0, 2, and 5 minutes and quenched with formic acid (final concentration of 5%) and analyzed by HPLC-MS using the method described below. Concentrations were calculated using a standard curve prepared in a solution of quenched, unreacted reaction mixture.

CETCH assays

Assay of CETCH

The initial photoCETCH cycle experiments were performed in 270 µl reaction volume with thylakoids added at 125 µg Chl/mL in a buffer containing: 50 mM HEPES, 330 mM Sorbitol, 10 mM sodium L-ascorbate, 100 µM coenzyme B_{12}, 80 µM propionyl-CoA, 1.25 mM ADP, 2 mM $NADP^+$, 5 mM $MgCl_2$, 5 mM K_2HPO_4, 10 mM KCl, 50 mM $NaH^{13}CO_3$, 1.2 µM catalase, 310 nM superoxide dismutase, 5 µM FdxCr, 1.3 µM Ghr, and the core enzymes from CETCH v6.0 (listed in Supplemental Table 3). Samples (30 µL) were taken at 0, 5, 15, 30, 45, 60, 90 and 120 minutes and quenched with formic acid at a final concentration of 5 %. The CoA esters were measured using an Agilent 6550 iFunnel Q-TOF LC-MS as described below. The glycolate produced was derivatized and measured by UPLC-MS/MS (using Agilent 6495B Triple Quad LC/MS) as described below. The glycolate was quantified using a standard curve. Standard solutions were prepared in a quenched, unreacted reaction mixture.

Assay of CETCH v6.0 with Ghr

CETCH cycle v6.0 was reacted in 300 µL with thylakoids added at 125 µg Chl/mL in a buffer containing: 50 mM HEPES-KOH, 330 mM Sorbitol, 10 mM sodium L-ascorbate, 100 µM coenzyme B_{12}, 80 µM propionyl-CoA, 1.25 mM ADP, 2 mM $NADP^+$, 5 mM $MgCl_2$, 5 mM K_2HPO_4, 10 mM KCl, 50 mM $NaH^{13}CO_3$, 1.2 µM catalase, 310 nM superoxide dismutase, 5 µM FdxCr, 1.3 µM Ghr, and the core enzymes from CETCH v6.0 (listed in Supplemental Table 3).

Samples (30 µL) were taken at 0, 5, 15, 30, 45, 60, 90 and 120 minutes and quenched with formic acid at a final concentration of 5 %. The CoA esters were measured using an Agilent 6550 iFunnel Q-TOF LC-MS as described below. The glycolate produced was derivatized and measured by UPLC-MS/MS (using Agilent 6495B Triple Quad LC/MS) as described below. The glycolate was quantified using standard curve. Solutions were prepared in a quenched, unreacted reaction mixture.

Assay of CETCH v7.0

CETCH cycle v7.0 was reacted in 300 µL with TEM added at 210 µg Chl/mL in a buffer containing: 50 mM HEPES-KOH, 700 mM Sorbitol, 10 mM sodium L-ascorbate, 100 µM coenzyme B_{12}, 85 µM propionyl-CoA, 0.5 mM ADP, 2 mM $NADP^+$, 5 mM $MgCl_2$, 5 mM K_2HPO_4, 10 mM KCl, 50 mM $NaH^{13}CO_3$, 1.2 µM catalase, 310 nM superoxide dismutase, 5 µM FdxCr, 1.3 µM Ghr, and the core enzymes from CETCH v7.0 (listed in Supplemental Table 3). Samples (30 µL) were taken at 0, 5, 15, 30, 45, 60, 90 and 120 minutes and quenched with formic acid at a final concentration of 5 %. The CoA esters were measured using an Agilent 6550 iFunnel Q-TOF LC-MS as described below. The glycolate produced was derivatized and measured by UPLC-MS/MS (using Agilent 6495B Triple Quad LC/MS) as described below. The glycolate was quantified using a standard curve. Standard solutions were prepared in a quenched, unreacted reaction mixture.

Optimization of CETCH v7.0 for droplets

CETCH cycle v7.0 was reacted in 300 µL with TEM added at 126 µg Chl/mL in a buffer containing: 50 mM HEPES-KOH, 700 mM Sorbitol, 10 mM sodium L-ascorbate, 85 µM crotonyl-CoA or propionyl-CoA, 0.5 mM ADP, 2 mM $NADP^+$, 5 mM $MgCl_2$, 5 mM K_2HPO_4, 10 mM KCl, 50 mM $NaH^{13}CO_3$, 1.2 µM catalase, 310 nM superoxide dismutase, 5 µM FdxCr, 1.3 µM Ghr, and the core enzymes from CETCH v7.0 (listed in Supplemental Table 3). Ecm and Mcm were incubated with 2 µl of a buffered solution of 5 mM coenzyme B_{12} for 30 minutes in the dark and at room temperature prior to adding the enzymes to the reaction mixture. Some samples included the addition of PhaJ (14 µM) and some reactions were incubated for 1 hour prior to illumination.

The samples (30 µL) were taken at 0, 5, 15, 30, 45, 60, 90 and 120 minutes and quenched with formic acid at a final concentration of 5 %. The CoA esters were measured using an Agilent 6550 iFunnel Q-TOF LC-MS as described below. The glycolate produced was derivatized and measured by UPLC-MS/MS (using Agilent 6495B Triple Quad LC/MS) as described below. The glycolate was quantified using a standard curve. Standard solutions were prepared in a quenched, unreacted reaction mixture.

Quantification of reaction products

High Resolution LC-MS/MS of CoA Esters

Compounds were separated on a RP-18 column (50 mm x 2.1 mm, particle size 1.7 µm, Kinetex EVO C18, Phenomenex) using a mobile phase system comprised of 50 mM ammonium formate pH 8.1 (A) and methanol (B). Chromatographic separation was carried out using the following gradient condition at a flow rate of 250 µL/min: 0 min 2.5% B; 2.5 min 2.5% B; 8 min 23% B; 10 min 80 %B; 11 min 80%; 12 min 2.5% B; 12.5 min 2.5% B. The column oven was set to 40 °C and autosampler was maintained at 10 °C. Standard injection volume was 1 µL.

CoA esters were analyzed using an Agilent 6550 iFunnel Q-TOF LC-MS system equipped with an electrospray ionization source set to positive ionization mode.

Capillary voltage was set at 3.5 kV and nitrogen gas was used as nebulizing (20 psig), drying (13 L/min, 225 °C) and sheath gas (12 L/min, 400°C). The TOF was calibrated using an ESI-L Low Concentration Tuning Mix (Agilent) before measurement (residuals less than 2 ppm for five reference ions) and was recalibrated during a run using 922 m/z as reference mass . The scan range for MS data is 500-1200 m/z.

Alternatively, the CoA esters were detected using an Agilent 6495B Triple Quad LC/MS system equipped with an electrospray ionization source. The source conditions were identical to that of the QTOF conditions. Data were acquired in the positive MRM mode with collision energy, dwell time, and fragmentor voltage set to 35 V, 20 ms, and 380 V respectively. The following MRM transitions were used to quantify the CoA esters : ethylmalonyl-CoA (882 m/z → 428 m/z and 331 m/z), methylsuccinyl-CoA (882 m/z → 428 m/z and 375 m/z), succinyl-CoA (868 m/z →

428 m/z and 361 m/z), methylmalonyl-CoA (868 m/z → 428 m/z and 317 m/z), propionyl-CoA (824 m/z → 428 m/z and 317 m/z), crotonyl-CoA (836 m/z → 428 m/z and 329 m/z), and β- / γ-hydroxybutyryl-CoA (854 m/z → 428 m/z and 347 m/z). To complement the MRM data, CoA esters were also UV detected at 260 nm on an Agilent 1290 Infinity II DAD detector equipped with a Max-Light cartridge cell (60 mm).

LC-MS data were analyzed using MassHunter Qualitative Navigator and QQQ Quantitative analysis software.

UPLC-MS/MS analysis of derivatized glycolate

Glycolate was derivatized according to the method published by Han et al. *(45)*. Briefly described, 50 µl of sample was mixed with 50 µL 150 mM 1-(3-Dimetheylaminopropyl)-3-ethylcarbodiimide (EDC), 50 µl 250 mM 3-nitrophenylhydrazine (3-NPH), and 50 µl of 7.5% pyridine in methanol in a 1.5 ml Eppendorf tube. The reaction was incubated at 30°C for 30 min. After incubation, the samples were centrifuged at 13,000 x *g* for 1 min and the supernatant transferred into HPLC vials.

UPLC-MS/MS analyses were performed on an Agilent 6495B Triple Quad LC/MS system equipped with an electrospray ionization source.

The analytes were separated on a RP-18 column (50 mm x 2.1 mm, particle size 1.8 µm, ZORBAX RRHD Eclipse Plus C18, Agilent) kept at 40 °C using a mobile phase system comprised of 0.1% formic acid in water (A) and acetonitrile (B). The gradient is as follows: 0 min 5% B; 1 min 5% B, 6 min 95% B; 6.5 min 95% B; 7 min 5 %B at a flow rate of 250 µL/min. Samples were held at 15°C and injection volume was 5 µL.

MS/MS data were acquired in negative MRM mode. Capillary voltage was set at 3 kV and nitrogen gas was used as nebulizing (25 psig), drying (11 L/min, 130 °C) and sheath gas (12 L/min, 400°C). The dwell time and fragmentor voltage were 20 ms and 380 V respectively. Optimized collision energy used for the both quantifier (210 *m/z* → 137 *m/z*) and qualifier (210 *m/z* → 152 *m/z*) and was 22 V.

LC-MS data were analyzed and quantified using MassHunter Qualitative Navigator and QQQ Quantitative Analysis softwares (Agilent).

UPLC-MS/MS analysis of ATP, ADP, and AMP

UPLC-MS/MS analyses were performed on an Agilent 6495B Triple Quad LC/MS system equipped with an electrospray ionization source.

The analyte was separated on a HILIC column (50 mm x 2.1 mm, particle size 1.7 µm, 130 Å, BEH Amide, Waters) using a mobile phase system comprised of 95:5 20 mM ammonium acetate pH 9.3 / acetonitrile (A) and acetonitrile (B). The compounds were eluted through the column at a flow rate of 400 µL/min under the following conditions: 0 min 90% B, 1.5 min 40% B, 1.8 min 40% B, 1.9 min 90 %B, 2.5 min 90% B. Samples were held at 15°C and injection volume was 1 µL.

MS/MS data were acquired in negative MRM mode. Capillary voltage was set at 3.5 kV and nitrogen gas was used as nebulizing (20 psig), drying (13 L/min, 225 °C) and sheath gas (12 L/min, 400°C). The dwell time and fragmentor voltage were 50 ms and 380 V respectively. Optimized collision energy used for the analytes were as follows: ATP (506 *m/z* → 408 *m/z*, 25 V, 506 *m/z* → 159 *m/z*, 35 V); ADP (426 *m/z* → 159 *m/z*, 25 V, 426 *m/z* → 79 *m/z*, 35 V); and AMP (346 *m/z* → 134 *m/z*, 35 V, 346 *m/z* → 79 *m/z*, 25 V).

LC-MS data were analyzed and quantified using MassHunter Qualitative Navigator and QQQ Quantitative Analysis softwares (Agilent).

Microfluidic device fabrication and operation

Dropmaker devices (fig. S8) were made of poly(dimethylsiloxane) (PDMS, Sylgard 184) from a SU8-3000 negative photoresist (MicroChem Corp) mold (30 µm depth) produced using a standard soft-lithography procedure (*46*). Microfluidic channels were treated using fluoro-silane (Aquapel, Aquapel) before use. Nemesys syringe pumps (Cetoni) were used to control the flows in the microfluidic channels. Devices were connected to pumps with PTFE tubing (Fischer

Scientific, ID 0.3 mm, OD 0.76 mm). Droplets were produced in fluorinated oil (Novec®3000, 3M) and stabilized against coalescence by a perfluoropolyether-polyethyleneglycol block-copolymer surfactant (Fluosurf, Emulseo).

A microfluidic 2D-chamber (fig. S8) was assembled as previously described (*10*). Briefly, the chamber geometry (35 mm x 10 mm) was cut in a 60 µm-thick double-sided bonding tape (1375, SDAG Adhésifs) using a Graphtech cutting plotter (CE 6000-40). The double-sided bounded template was sandwiched between two microscopy glass slides (76 x 25 x 1mm, Mareinfeld). Holes and glued nanoports on the top glass slide served as inlet/outlet. The chambers were treated using fluoro-silane (Aquapel, Aquapel) before use.

Thylakoid encapsulation

Independently from final composition, thylakoids suspensions were flowed (100 µL/h) in the dropmaker device and flow-focused with two streams of fluorinated oil containing 3 wt% surfactant (225 µL/h). In typical experiments, 4-bit emulsions were produced by encapsulating four different mixtures in parallel. The 4-bit emulsions were barcoded with sulforhodamine B fluorophore (2, 8, 16, 40 µM). Droplets were collected together in a PTFE tubing and directed to the 2D-chamber. Once the 2D-chamber was fully loaded, flows were stopped and the 2D-chamber closed with caps. Specific assay mixtures can be found in the tables below.

Time-lapse fluorescence measurements

The 2D-chamber device was mounted on the stage of an inverted microscope equipped with light emitting diodes (fig. S8). A 365 nm diode (1150 mW, Thorlabs) combined to an epifluorescence cube composed of an excitation bandpass filter (F39-370, AHF), a beamspliter (F38-409, AHF) and an emission bandpass filter (F39-438, AHF) was used for measuring NADPH fluorescence. A 550 nm diode (CoolLED pE-2) was used for measuring sulforhodamine B

fluorescence. A warm white light emitting diode (2000 mW, Thorlabs) mounted on the stage of the microscope was used for the light-activation of the thylakoids. Images were taken with a digital camera (EOS 600, Canon). A labVIEW routine triggering the white LED, the 365 nm LED, and the digital camera was used to perform the time lapse experiments with defined light and imaging patterns.

Image processing

The home-made image processing algorithm consists of a three-step procedure to automatically extract information from every image captured during the time-lapse experiment (fig. S9). (i) A region of interest is drawn on the brightfield image to select the droplets of interest and discard droplets located in the image corners. Using the brightfield image, an intensity threshold is applied in order to discriminate the edges of the droplets to the background of the image. Then, the brightfield image is converted into a binary image where the edges of the droplets are only displayed. From this binary image, droplet boundaries are detected using the Hough transform procedure. The detection of droplets is limited to the range of a low and high radius in order to reduce the time processing. The Hough transform procedure outputs radius and the locations of droplets in the region of interest. The data are saved and the image processing algorithm automatically moves to the coding image. (ii) The coding image is captured at the same location as the brightfield image. Consequently, the droplet location and radius data can be used to find every droplet of interest in the coding image. The fluorescence intensity of each droplet is obtained by listing the intensity value of all pixels composing the droplets tested. The median value of the pixel intensity for each droplet is saved and characterizes the coding intensity of the droplet tested. This process is repeated for every droplet in the imaged region of the interest. Then the image processing algorithm moves to the time lapse images. (iii) Every time lapse image is processed using the same method as the coding image step (ii). Briefly, the median value of the fluorescence intensity of every pixel composing a droplet is saved. Then, this process is iterated for every droplet and image composing the time lapse. The LabVIEW code used for image analysis has been uploaded to a repository on GitHub (*34*).

Large-scale experiments

1-bit emulsions (contents outlined below) were produced in large quantities (~500 µL, ~10^8 droplets) and collected in a 2 mL glass vial. The glass vial was continuously rotated and illuminated with warm white LED. 30 µL of emulsion was regularly sampled from the vial and coalesced as follows: the droplets were added to 50 µL of fluorinated oil; 20 µL of 1H, 1H, 2H, 2H-perfluoro-1-octanol was added and the mixture was vortexed and centrifuged; and the aqueous phase was pipetted and quenched with 1% of HCl.

Ccr and Ghr in 1-bit emulsions

TEM powered reactions Ghr and Ccr in droplets were assayed in a buffer containing the following: 100 mM HEPES-KOH, pH 7.8, 330 mM sorbitol, 5 mM K_2HPO_4, 10 mM KCl, 5 mM $MgCl_2$, 10 mM sodium L-ascorbate, 5 µM ferredoxin, 52 U mL^{-1} superoxide dismutase, 1.2 µM catalase, 1.6 mM ADP, 0.8 mM $NADP^+$, 120 µg Chl mL^{-1} of TEM, and 8 µM Sulforhodamine B. To assay Ccr: 255 nM Ccr, 33.5 nM carbonic anhydrase, 1 mM Crotonyl-CoA, and 50 mM $NaHCO_3$ was added. To assay Ghr: 214 nM GhrB and 5 mM glyoxylate was added. Droplets were created from a solution with a total volume of 500 µL. Samples were taken after 75 minutes of illumination at 50 µmol photons m^{-2} s^{-1} and quenched as described above. To assess Ccr activity CoA-thioesters were measured by HPLC-MS as described above and quantified using a standard curve. Ghr activity was assessed by measuring glycolate produced by HPLC-MS. The concentration was determined using a standard curve. Standard solutions were prepared in a buffer reflective of assay conditions for accurate concentration calculation.

1-bit emulsions containing CETCH v7.0 and TEM

Droplets containing TEM powered CETCH v7.0 were generated from a solution (total volume, 1.8 mL) that contained 70 µg Chl/mL in a buffer that contained 50 mM HEPES-KOH,

pH 7.8, 700 mM Sorbitol, 10 mM sodium L-ascorbate, 90 µM crotonyl-CoA, 0.5 mM ADP, 2 mM $NADP^+$, 5 mM $MgCl_2$, 5 mM K_2HPO_4, 10 mM KCl, 50 mM $NaH^{13}CO_3$, 10 mM polyphosphate, 1.2 µM catalase, 310 nM superoxide dismutase, 5 µM FdxCr, 1.3 µM GhrA, 14 µM PhaJ, and the core enzymes from CETCH v7.0 (listed in Supplemental Table 3). Ecm and Mcm were incubated with 2 µl of a buffered solution of 5 mM coenzyme B_{12} for 30 minutes in the dark and at room temperature prior to adding the enzymes to the reaction mixture. The samples (30 µL) were taken and quenched as described above. The CoA esters were measured using an Agilent 6550 iFunnel Q-TOF LC-MS and quantified using the integrated UV_{260nm} peak and a standard curve. The glycolate produced was derivatized and measured by UPLC-MS/MS (using Agilent 6495B Triple Quad LC/MS) as described above.

Thylakoid activity in droplets 2, 3, & 4-bit emulsions

Thylakoid Stability

Thylakoid stability was assayed (fig. S11B). Four populations of droplets were created from 0.4 mL solutions that contained 50 mM HEPES-KOH, pH 7.8, 700 mM sorbitol, 5 mM K_2HPO_4, 10 mM KCl, 5 mM $MgCl_2$, 10 mM sodium L-ascorbate, 5 µM Ferredoxin, 52 U mL^{-1} superoxide dismutase, 1.2 µM catalase, 1.6 mM ADP, and various concentrations of sulforhodamine B, thylakoids, NADPH, and $NADP^+$. Population 1 contained: 0.8 mM $NADP^+$, 33 µg Chl mL^{-1}, 2 µM sulforhodamine B. Population 2 contained: 0.8 mM $NADP^+$, 65 µg Chl mL^{-1}, 8 µM sulforhodamine B. Population 3 contained: 0.8 mM $NADP^+$, 130 µg Chl mL^{-1}, 16 µM sulforhodamine B. Population 4 contained: 0.8 mM NADPH, 0 µg Chl mL^{-1}, 40 µM sulforhodamine B. Droplets were prepared and monitored as discussed above.

Controlling TEM in droplets with fluctuating light conditions

The effect of fluctuating light conditions in the droplets was tested (fig. S13). Three populations of droplets were created from 0.5 mL solutions that contained: 50 mM HEPES-KOH, pH 7.8, 330 mM sorbitol, 5 mM K_2HPO_4, 10 mM KCl, 5 mM $MgCl_2$, 10 mM sodium L-ascorbate, 5 µM Ferredoxin, 52 U mL^{-1} superoxide dismutase, 1.2 µM catalase, 0.8 mM ADP, and various

concentrations of sulforhodamine B, thylakoids, NADPH, and $NADP^+$. Population 1 contained: 0 μg Chl mL^{-1} of thylakoids, 0.5 mM $NADP^+$, 2 μM sulforhodamine B. Population 2 contained: 11 μg Chl mL^{-1} of thylakoids, 0.5 mM $NADP^+$, 8 μM sulforhodamine B. Population 3 contained: 0 μg Chl mL^{-1} of thylakoids, 0.5 mM NADPH, 40 μM sulforhodamine B. Droplets were prepared and monitored as discussed above.

Light intensity

The effect of light intensity in NADPH production on the droplets was assayed using light intensities at 50, 100, 200, 400 and 1200 μmol photons m^{-2} s^{-1} (fig. S12). Two populations of droplets were created from solutions of 0.5 mL that contained: 100 mM HEPES-KOH, pH 7.8, 330 mM sorbitol, 3 mM K_2HPO_4, 10 mM KCl, 5 mM $MgCl_2$, 10 mM sodium L-ascorbate, 5 μM Ferredoxin, 52 U mL^{-1} superoxide dismutase, 1.2 μM catalase, 0.75 mM ADP, and various concentrations of sulforhodamine B, thylakoids, NADPH, and $NADP^+$. Population 1 contained: 23 μg Chl mL^{-1} of thylakoids, 0.5 mM $NADP^+$, 2 μM sulforhodamine B. Population 2 contained: 0 μg Chl mL^{-1} of thylakoids, 0.5 mM NADPH, 40 μM sulforhodamine B.

Thylakoid consistency in droplets

The consistency between independently prepared droplets was tested using droplets manufactured from four independently pipetted 0.5 mL solutions (fig. S9C & S10C). The four populations contained: 50 mM HEPES-KOH, pH 7.8, 700 mM sorbitol, 5 mM K_2HPO_4, 10 mM KCl, 5 mM $MgCl_2$, 10 mM sodium L-ascorbate, 5 μM Ferredoxin, 52 U mL^{-1} superoxide dismutase, 1.2 μM catalase, 1.6 mM ADP, and various concentrations of sulforhodamine B, thylakoids, NADPH, and $NADP^+$. Population 1, 2, and 3 contained: 1.0 mM $NADP^+$, 125 μg Chl mL^{-1} of thylakoids, and either 2, 8, 20 μM sulforhodamine B. In population 4, thylakoids were omitted and 1 mM NADPH was used instead of $NADP^+$, for the coding dye 40 μM was used. Droplets were prepared and monitored as discussed above.

Controlling Droplets

Various enzyme and substrate concentrations were used in multiplexed experiments (4-bit, Fig. 3E, S14B, & S14C). In each case the TEM was coupled to Ghr and either various enzyme and/or substrate concentrations were assayed. The specific reaction conditions are shown in Table S4. The droplets were manufactured and monitored as discussed above from 0.5 mL solutions.

Ghr and Ccr in droplets

Both 330 and 700 mM sorbitol conditions were tested with coupling Ccr and Ghr. In each case, four populations were tested either with 330 or 700 mM sorbitol (Fig. 3F, S14D, & S15B). The specific reaction conditions are shown in Table S5. The droplets were manufactured and monitored as discussed above from 0.5 mL solutions. The contents of each droplet population is indicated and a grey box indicates that component was omitted from that population.

Pcs in droplets

The specific reaction conditions to test Pcs coupling is shown in Table S6 (fig. S16). The four populations of droplets were manufactured and monitored as discussed above from 0.5 mL solutions. The contents of each droplet population is shown and a grey box indicates that component was omitted from that population.

Time and space control of droplets 2-bit emulsion

As a demonstration of the controllability of droplets, both in time and space, a binary emulsion was created (Fig. 3G). The two population of droplets were created using 0.5 mL solutions. The two populations contained 50 mM HEPES·KOH, pH 7.8, 700 mM sorbitol, 5 mM K_2HPO_4, 10 mM KCl, 5 mM $MgCl_2$, 10 mM sodium L-ascorbate, 5 μM Ferredoxin, 52 U mL^{-1} superoxide dismutase, 1.2 μM catalase, 1.2 mM ADP, 0.8 mM $NADP^+$, 10 mM glyoxylate, and two different concentrations of GhrA, thylakoids, or sulforhodamine B. Either: 40 nM GhrA, 200 μg Chl mL^{-1} thylakoids, and 2 μM sulforhodamine B or 2.5 nM GhrA, 40 μg Chl mL^{-1}thylakoids, and 8 μM sulforhodamine B.

The 2 populations of droplets were filled into the observation chamber via two inlets. After 2 minutes in the dark, the droplets were exposed to 50 µmol photons m^{-2} s^{-1} light. The light was turned off again after 60 minutes.

CETCH in droplets

Four-bit reaction conditions for droplets containing CETCH v6.0 and 7.0 that were monitored in the 2D array chamber described in Table S7 (Fig 4B, 4C, S18A & S18B). Three experiments are shown and droplets were created from 500 µL solutions. The contents of each droplet population is shown and a grey box indicates that component was omitted from that population.

Movie S1.

Time-lapse of $NADP^+$ photoreduction in droplets containing various concentrations of TEM (experiment shown in **Fig. 3B**). Images show NADPH fluorescence, excited using a 365 nm diode, images taken every 2.5 minutes.

Movie S2.

Time-lapse of NADPH oscillations in light/dark cycles of droplets containing the Ghr reaction (experiment shown in **Fig. 3F**). Images show NADPH fluorescence, excited using a 365 nm diode, images taken every 2.5 minutes.

Movie S3.

Time-lapse of NADPH fluorescence of experiment demonstrating how the metabolic activity of droplets can be controlled in time and space (experiment shown in **Fig. 3G**). Images show NADPH fluorescence, excited using a 365 nm diode. After 2 minutes in the dark, the droplets were exposed to 50 µmol photons m^{-2} s^{-1} light. The light was turned off again after 60 minutes. The images were taken every minute for the first 5 minutes, at 7.5 minutes, then every 5 minutes until 125 minutes, and taken every 10 minutes after that.

Movie S4.

Time-lapse of the NADPH fluorescence of droplets encapsulated with variations of the full CETCH cycle (experiment shown in **Fig. 4B & C,** detailed droplet contents can be found in Table S7). Images show NADPH fluorescence, excited using a 365 nm diode. The images are taken every 2.5 minutes.

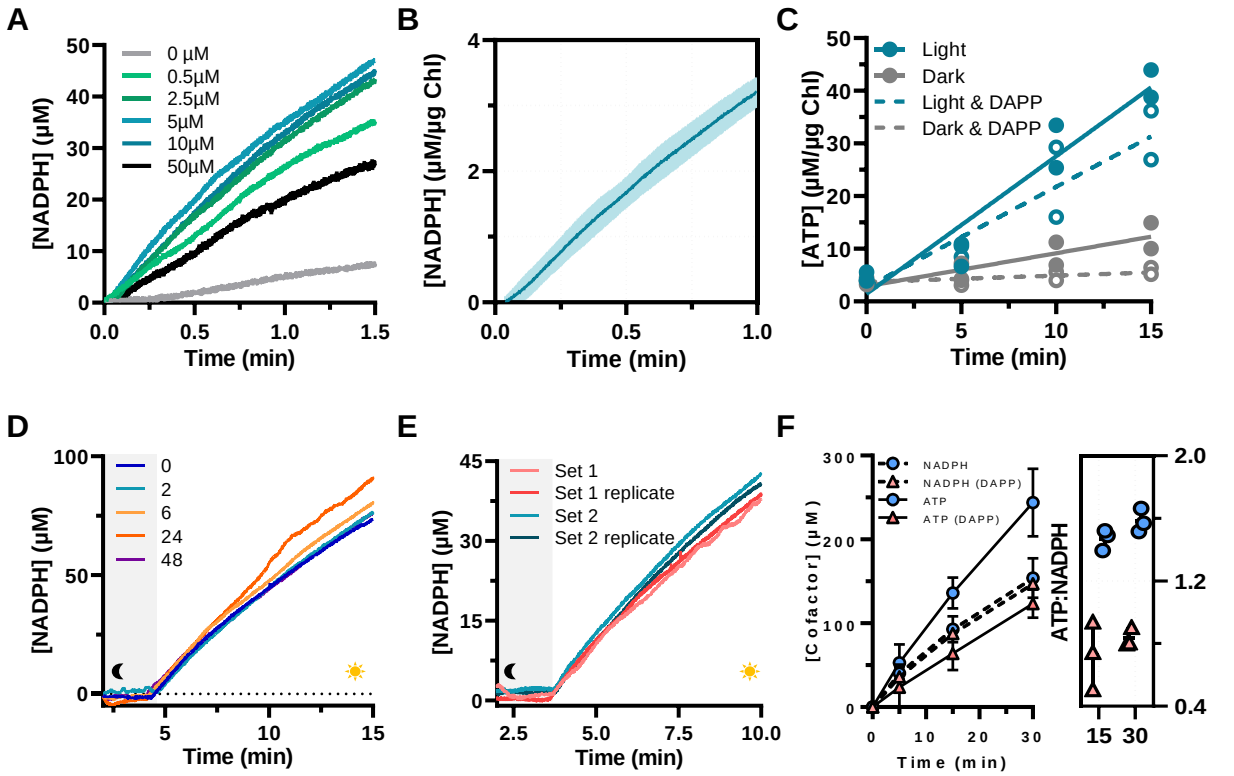

Fig. S1. Characterization, stability and stoichiometry of light-driven ATP and NADPH regeneration by thylakoid membrane-based energy modules (TEMs).
(**A**) $NADP^+$ photoreduction: Titration of ferredoxin concentrations. NADPH production is dependent upon the addition of external ferredoxin. The highest rates of $NADP^+$ photoreduction were achieved with the addition of ferredoxin between 2.5-10 µM. Shown are representative examples of NADPH production rates at 100 µmol photons m^{-2} s^{-1}, 10 µg total chlorophyll a + b (Chl) and varying ferredoxin concentrations. (**B**) $NADP^+$ photoreduction by photosynthetic membranes NADPH production rate normalized to µg of Chl (line is the mean value with shaded area corresponding to ± standard deviation, N = 6). Rate of $NADP^+$ photoreduction was determined from the first minute after the light had been turned on (100 µmol photons m^{-2} s^{-1}). (**C**) Light-driven ATP formation and dark-control in the presence of the adenylate kinase inhibitor DAPP (teal and grey, respectively; open circles indicate samples with DAPP added). The addition of DAPP decreases ATP formation both in the dark and in the light (lines shown are linear fits, 2 biological replicates, 60-70 µmol photons m^{-2} s^{-1}), presumably due to inhibition of the background reaction of membrane-bound adenylate kinase. (**D**) Stability of TEMs in the dark: NADPH production of TEM were maintained in the dark for 1 and 2 hours (at room temperature) or 6, 24, and 48 hours, respectively (at 0 ℃, 60 µmol photons m^{-2} s^{-1}). (**E**) Reproducibility of TEM preparations: NADPH production rates of TEMs are consistent between different thylakoid preparations. Two replicate experiments from two different thylakoid preparations are shown (at 23 ℃, 60 µmol photons m^{-2} s^{-1}). (**F**) Stoichiometry of cofactor regeneration: ATP (solid lines) and NADPH (dashed lines) production in the presence (coral triangles) and absence of DAPP (blue circles), and the calculated ATP to NADPH ratio at 15 and 30 minutes after light exposure (60 µmol photons m^{-2} s^{-1}).

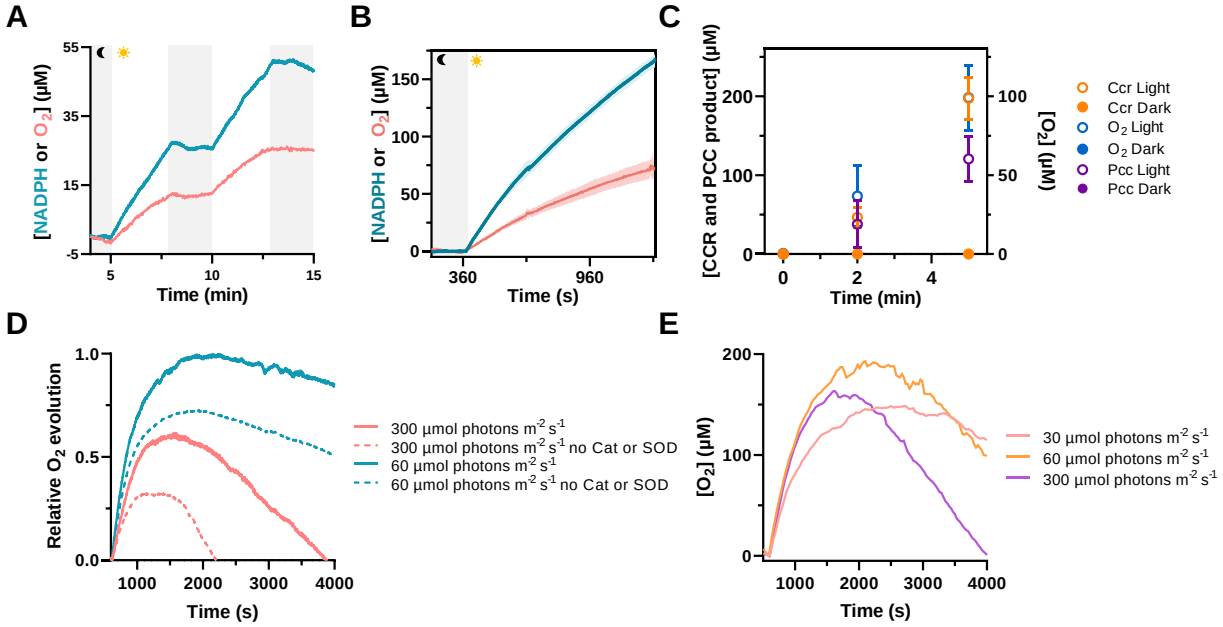

Fig. S2. Oxygen evolution

(**A**) Relative molar $NADP^+$ photoreduction and O_2 evolution curves over light/dark cycles. The O_2 production occurs in a 1:2 molar ratio with NADPH, the same ratio that occurs under physiological conditions. (**B**) NADPH production with O_2 evolution curves at 60 µmol photons m^{-2} s^{-1}. Lines are the average of three replicates and the standard deviation is shown in the shaded area. (**C**) Product formation from Ccr and Pcc alongside the O_2 evolution measurements. (**D**) Relative O_2 evolution at 60 or 300 µmol photons m^{-2} s^{-1} in a reaction buffer either with or without catalase (Cat) and superoxide dismutase (SOD). (**E**) A similar experiment as in (**D**) but an even lower light condition is shown. All conditions contained SOD and catalase. At 30 µmol m^{-2} s^{-1} the O_2 evolution was slower but was maintained longer.

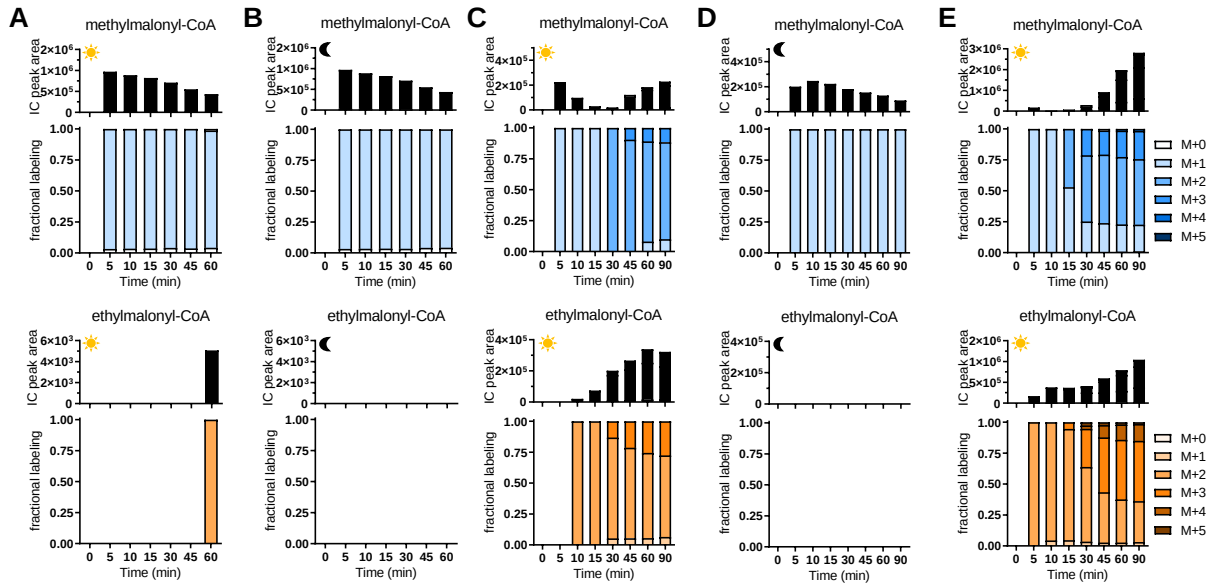

Fig. S3. Initial experiments to couple the CETCH cycle to TEM (in bulk).

To couple the CETCH cycle to TEM, enzymes of the CETCH cycle plus Ghr from *E. coli* were mixed with TEM. Propionyl-CoA was added and the reaction mixture was illuminated (100 µmol photons m^{-2} s^{-1}). Operation of the CETCH cycle was assessed by following the ^{13}C-labelling patterns (see fig. S4) and CETCH cycle metabolites methylmalonyl-CoA and ethylmalonyl-CoA as previously described *(2)*. (**A**-**B**) Labelling pattern of CETCH v6.0 coupled to TEM (50 µg Chl mL^{-1}) starting with 150 µM propionyl-CoA. Both conditions were supplemented with an addition of 10 µM ferredoxin-$NADP^+$ reductase (FNR), with added 15 µM FAD (1:1.5 molar ratio, for the contribution of FAD and FNR on the system, see fig. S6). Very little difference between the light (**A**) and dark (**B**) operated cycles was observed and ethylmalonyl-CoA was only detected after 60 minutes in the light and not detected in the dark. (**C**-**D**) Labelling pattern of CETCH v6.0 coupled to TEM (70 µg Chl mL^{-1}) in the absence of FNR starting with 150 µM propionyl-CoA (see fig. S6 for details on the effect of FNR and its interplay with Mco and free FAD). When additional FNR was left out of the reaction mixture, the cycle operation increased under illumination (**C**), demonstrated by the ^{13}C-labelling pattern and formation of ethylmalonyl-CoA. The dark control (**D**) did not show any significant label incorporation and no ethylmalonyl-CoA formation. (**E**) Positive control demonstrating that supernatant of a TEM reaction (with 20 µg Chl) illuminated for 45 minutes is able to provide sufficient NADPH and ATP to subsequently operate the CETCH cycle v6.0 for several rounds, suggesting some negative interactions of CETCH cycle v5.4 and TEM.

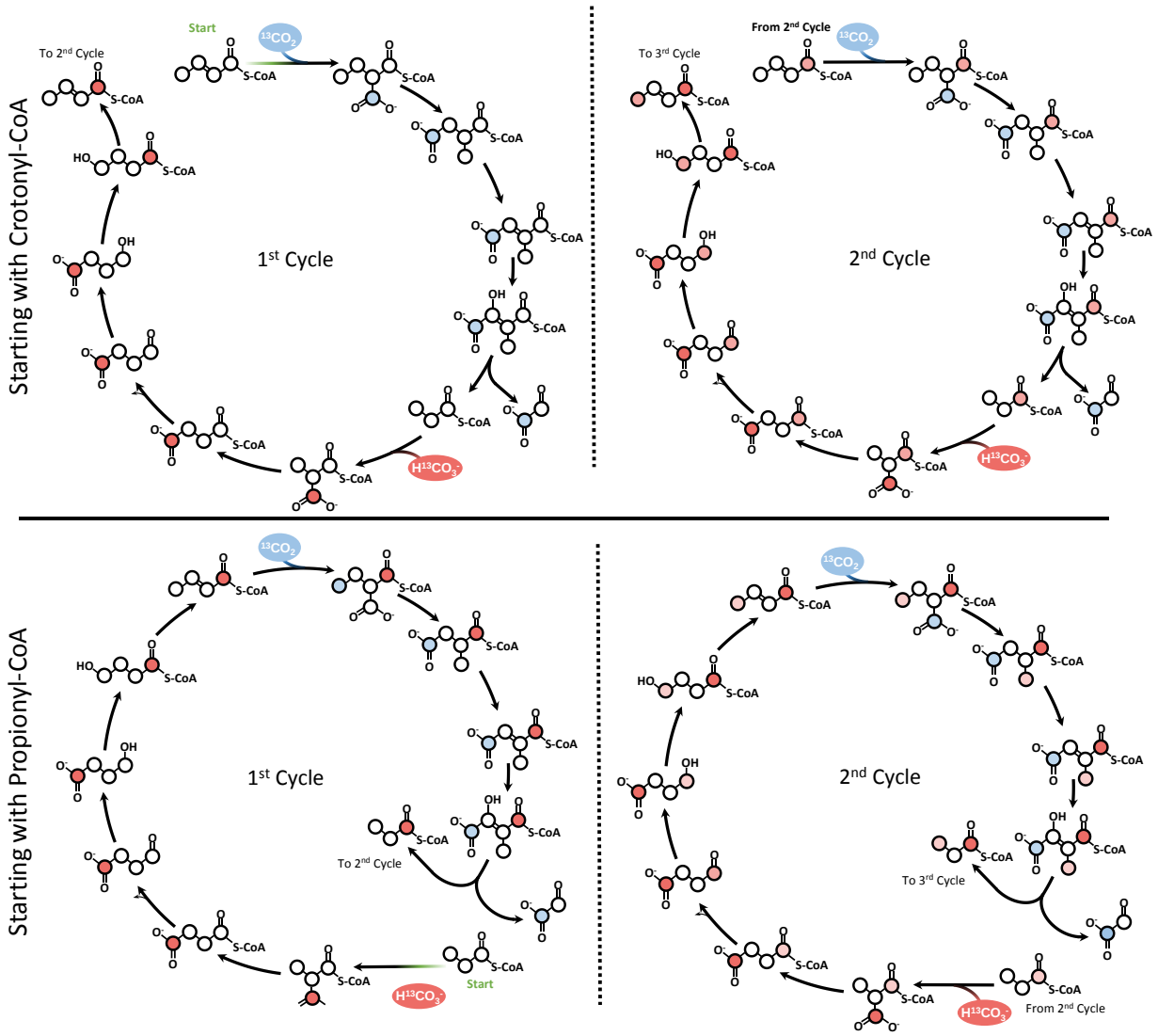

Fig. S4. Expected $^{13}CO_2$ isotopic labelling pattern in the CETCH cycle

Shown is the expected labelling pattern for the first two turns of the CETCH cycle starting at either crotonyl-CoA or propionyl-CoA using isotopic labelling with ^{13}C-bicarbonate. The cycle features two CO_2-incorporation steps per turn catalyzed by Ccr (shown in blue) and Pcc (shown in red). ^{13}C-labeled carbon incorporated into the C4-acceptor crotonyl-CoA by Ccr remain with the output molecule glyoxylate when β-methylmalyl-CoA is split by Mcl into propionyl-CoA and glyoxylate (position and migration of the ^{13}C-label is shown in blue). The carbon incorporated into the C3-acceptor propionyl-CoA (shown in red) stays with the acceptor molecule during each turn of the cycle (position and migration of the ^{13}C-label is indicated by different shades of red). Note that the CETCH cycle includes carbon skeleton-rearranging steps catalyzed by mutases, resulting in a complex labelling pattern.

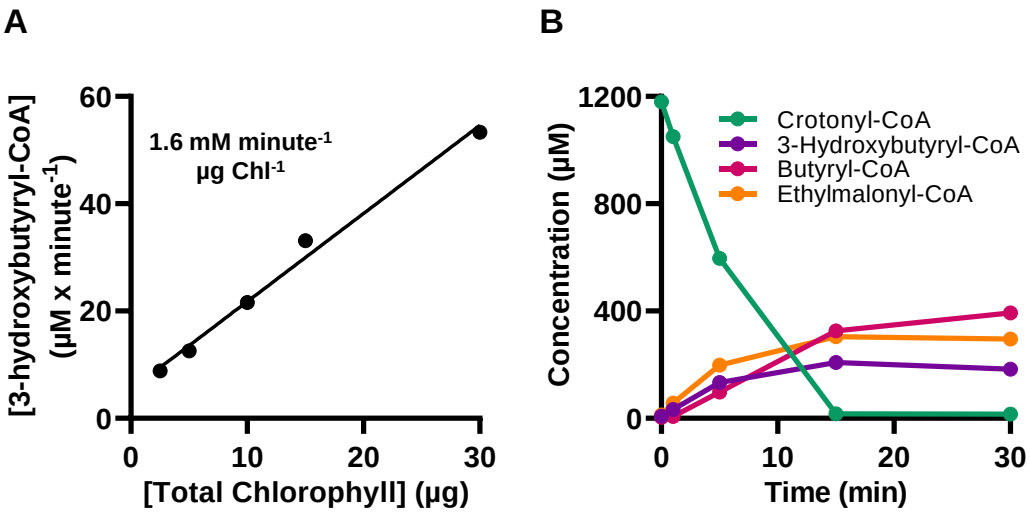

Fig. S5. 3-hydroxybutyryl-CoA formation by TEMs

(**A**) Incubation of TEM with 1.2 mM crotonyl-CoA in the dark leads to formation of 3-hydroxybutyryl-CoA. 3-Hydroxybutyryl-CoA formation is light-independent and linear to the TEM concentration at a rate of 1.6 ± 0.1 µM minute^{-1} µg^{-1} Chl (Y = 1.642X + 5.356, R^2 = 0.99) The reaction mixture included 5 µM Fdx, 310 nM SOD, 1.2 µM Cat, 1.85 µM Pcc, and 1.29 µM Ccr and various concentrations of TEM (2.5, 5, 10, 15, and 30 µg Chl). (**B**) The same reaction conditions but under illumination (60 µmol photons m^{-2} s^{-1}) and in the presence of Ccr (1.29 µM). TEM-dependent conversion of crotonyl-CoA (green) into 3-hydroxybutyryl-CoA (purple) is still significant compared to the conversion catalyzed by Ccr (orange). Shown is a reaction containing 10 µg Chl.

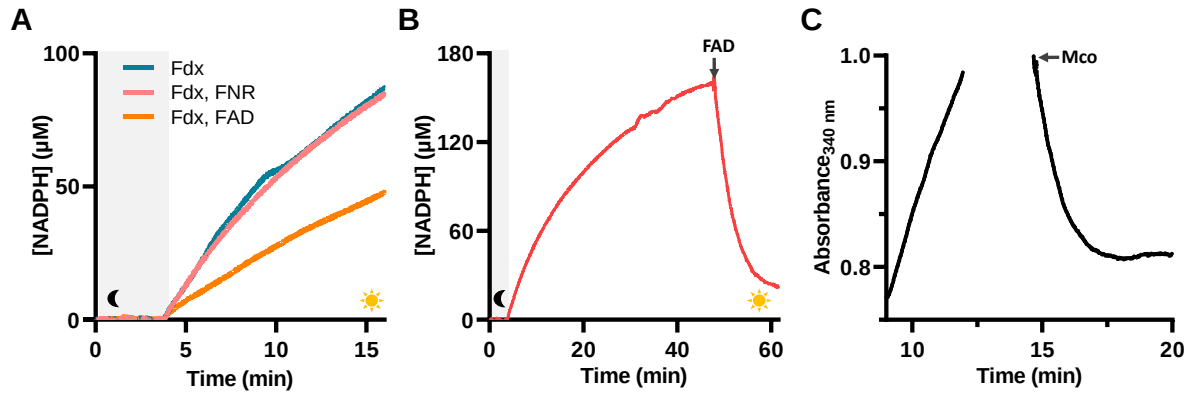

Fig. S6. Negative effect of Mco and free FAD on NADP$^+$-dependent photoreduction by TEM

(**A**) NADP$^+$ photoreduction monitored on a spectrophotometer at 340 nm by TEM starts upon illumination (60 µmol photons m^{-2} s^{-1}). Fdx is required for NADP$^+$ photoreduction (fig. S1A) and adding 5 µM FNR did not improve the NADPH production rate from TEM (10.3 µM min^{-1} with only Fdx and 9.9 µM min^{-1} with Fdx and FNR, calculated from the first 2.5 minutes of illumination). However, adding excess FAD (14 µM) decreases this rate (4.3 µM min^{-1}). **(B)** NADPH is produced in the presence of FNR and Fdx (5 µM each) but inhibited upon the addition of FAD (14 µM) even under constant illumination. **(C)** NADPH production in the presence of FNR is inhibited by addition of Mco with excess FAD (10.5 and 15 µM, respectively). In summary, this shows that free FAD via FNR directly interferes with NADPH productivity of TEMs. Optimization of assay conditions, implementation of wild type enzymes (Mcd) that bind FAD tighter, or circumventing FAD-dependent transformations entirely are critical for coupling the CETCH cycle to TEMs.

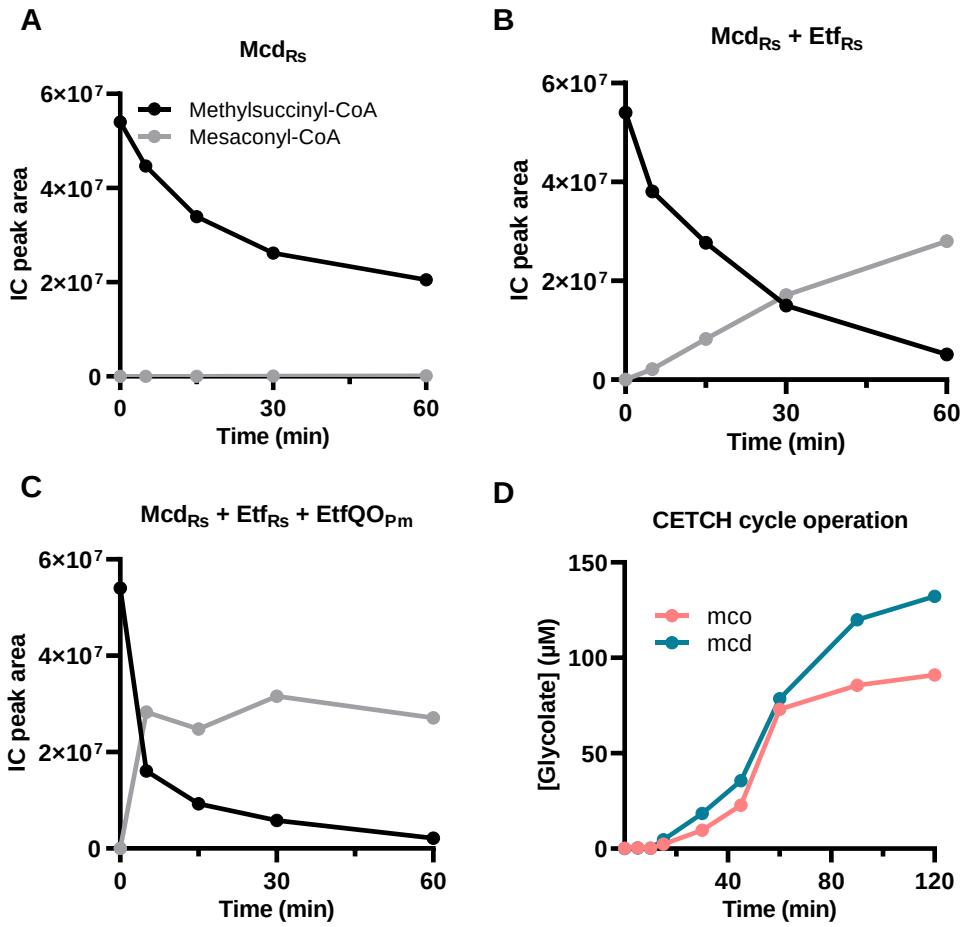

Fig. S7. Developing a functional Mcd reaction for CETCH v7.0.

In natural systems, the conversion of methylsuccinyl-CoA to mesaconyl-CoA is catalyzed by Mcd. Mcd is a FAD–dependent acyl-CoA dehydrogenase, which is coupled via electron transfer flavoproteins (Etf) to the membrane-located ubiquinone pool. During the development of the CETCH cycle Mcd alone and in combination with its cognate Etf was not sufficient to operate the CETCH cycle *(2)*. This required engineering of a Mco that was ultimately used in CETCH v5.4. Mco can impair TEM productivity through ROS and free FAD (fig. S5A) and therefore, we aimed to replace Mco in the CETCH cycle with a functional Mcd reaction. (**A**) Mcd (6.75 µM**)** from *Rhodobacter sphaeroides* (Mcd_{Rs}) alone does not catalyze the conversion of methylsuccinyl-CoA (starting with 250 µM, shown in black) into mesaconyl-CoA (grey). The decrease of methylsuccinyl-CoA in the reaction mixture is due to spontaneous CoA-thioester hydrolysis. (**B**) Mcd in combination with 6.25 µM of its cognate Etf from *R. sphaeroides* (Etf_{Rs}) is able to form mesaconyl-CoA, likely due to re-oxidation of Etf in the presence of O_2. (**C**) Addition of 6.25 µM Etf-ubiquinone oxidoreductase from *Pseudomonas migulea* ($EtfQO_{Pm}$) increases the conversion of methylsuccinyl-CoA into mesaconyl-CoA by Mcd_{Rs} and Etf_{Rs} more than tenfold. (**D**) Replacing Mco in CETCH v6.0 with Mcd_{Rs}, Etf_{Rs}, and $EtfQO_{Pm}$ (3, 8, and 1 µM respectively) creates CETCH v7.0. Comparison of glycolate formed from CETCH v6.0 (Mco-based) and CETCH v7.0 (Mcd-Etf-EtfQO-based) using Ppk and Fdh as regeneration systems and starting with 2 mM $NADP^+$ and 0.5 mM ADP.

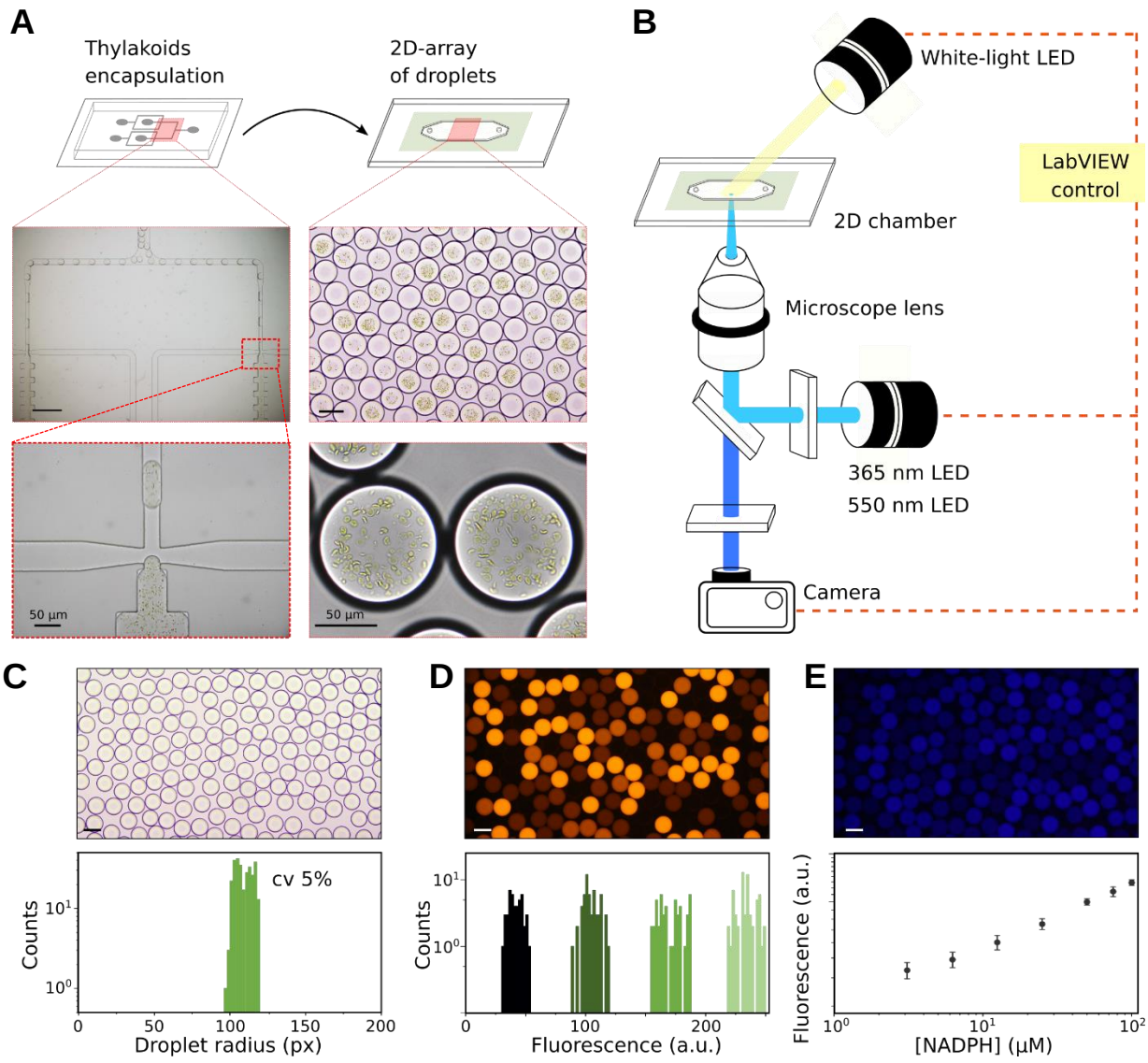

Fig. S8. Description of the microfluidic platform.

(**A**) Microfluidic workflow. Thylakoids are encapsulated in 300 pL water-in-oil (w/o) droplets using a dropmaker device with two parallel production nozzles (30x30 µm). Two devices are used in parallel to produce 4-bit emulsions. Droplets are then flowed into an incubation chamber and stored as a 2D-array for light activation and time-lapse microscopy imaging. (**B**) Optical setup. The 2D-incubation chamber is integrated on the stage of an inverted microscope equipped with a 10x objective. A white-light LED and a 365 nm LED are used for the light activation of the thylakoids and the NADPH fluorescence excitation, respectively. The two LEDs are triggered together with the camera using a home-made LabVIEW routine to perform automated time-lapse fluorescence imaging with defined light/dark cycles. A 550 nm LED is used for the sulforhodamine B fluorescence excitation (barcoding). (**C**) Bright-field image of a 4-bit emulsion and droplet radius distribution. (**D**) 550 nm (barcoding) fluorescence image and droplet fluorescence distribution. (**E**) 365 nm (NADPH) fluorescence image. Linear relationship between NADPH concentration and 365 nm fluorescence. Scale bars are 100 µm unless specified.

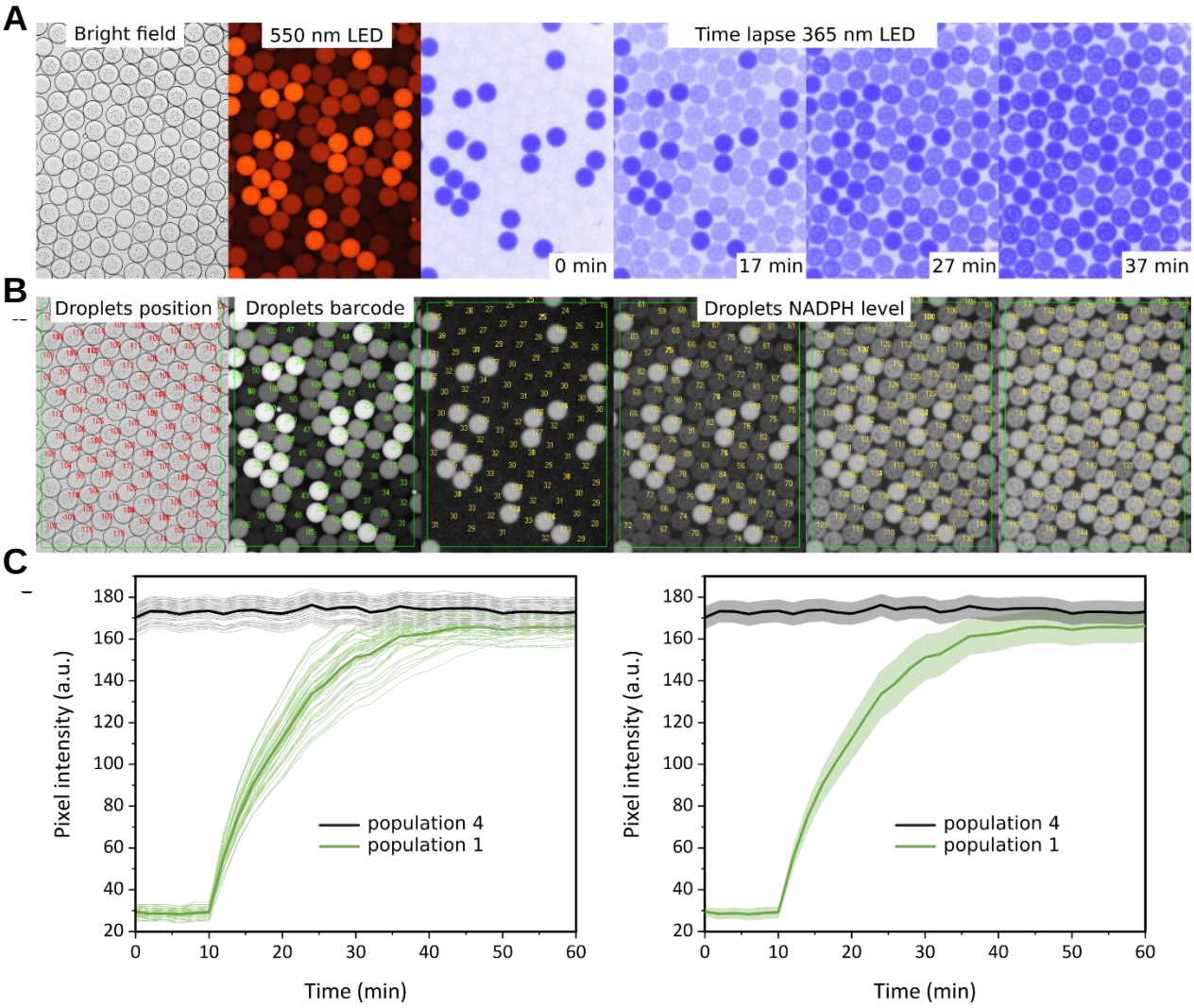

Fig. S9. Image processing workflow.

(**A**) Typical sequence of processed images: bright-field, 550 nm LED and 365 nm LED time-lapse images (0, 17, 27 and 37 min). Scale bars are 100 µm. (**B**) Image processing of the sequence. A region of interest is defined. Droplet positions and radii are extracted from the bright-field image. The 4-bit droplet barcoding is extracted from the 550 nm fluorescence image. The NADPH level of each droplet over time is extracted from the 365 nm fluorescence time-lapse imaging. (**C**) Dynamics of NADPH concentration at the single droplet level are shown by 365 nm fluorescence versus time for each individual droplet. The mean for each population is indicated in bold. In a typical experiment, N = 50 for each population. For more clarity, only population 1 and population 4 are shown here. On the right, the average of the same populations is shown with the corresponding standard deviation indicated by the shaded area.

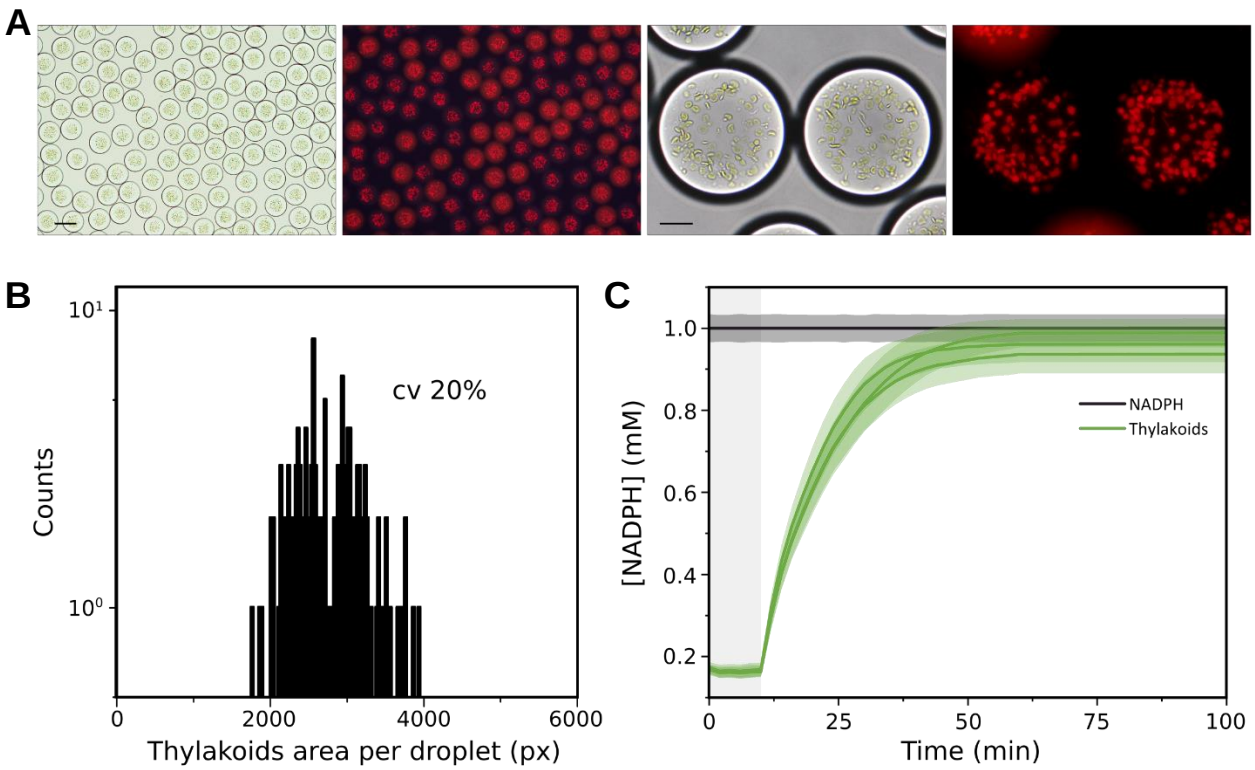

Fig. S10. TEM encapsulation.

(A) Bright-field and chlorophyll fluorescence images of thylakoids within 300 pL w/o droplets. Scale bars are 100 µm. **(B)** Distribution of the thylakoids: area per droplet estimated using image processing. Briefly, similar to the time-lapse algorithm, the Hough transform procedure is used on binary images to detect droplet boundaries. Then, a local threshold intensity allows the detection of thylakoids in the droplet. This step is suitable to distinguish thylakoids with a low intensity from the image background. Finally, the pixels identified as thylakoids in the droplet are summed. This process is iterated for every droplet. **(C)** NADPH production consistency. NADPH concentration over time for three different droplets populations prepared with the same initial quantity of added thylakoids normalized by total chlorophyll (125 µg Chl mL^{-1}) and containing 1 mM $NADP^+$ under continuous illumination (50 µmol photons m^{-2} s^{-1}). NADPH concentration of all populations was corrected for the non-catalytic oxidation observed in the NADPH-only control. The average measurements are indicated by a bold line with corresponding shading indicating the ± standard deviation (N = 50).

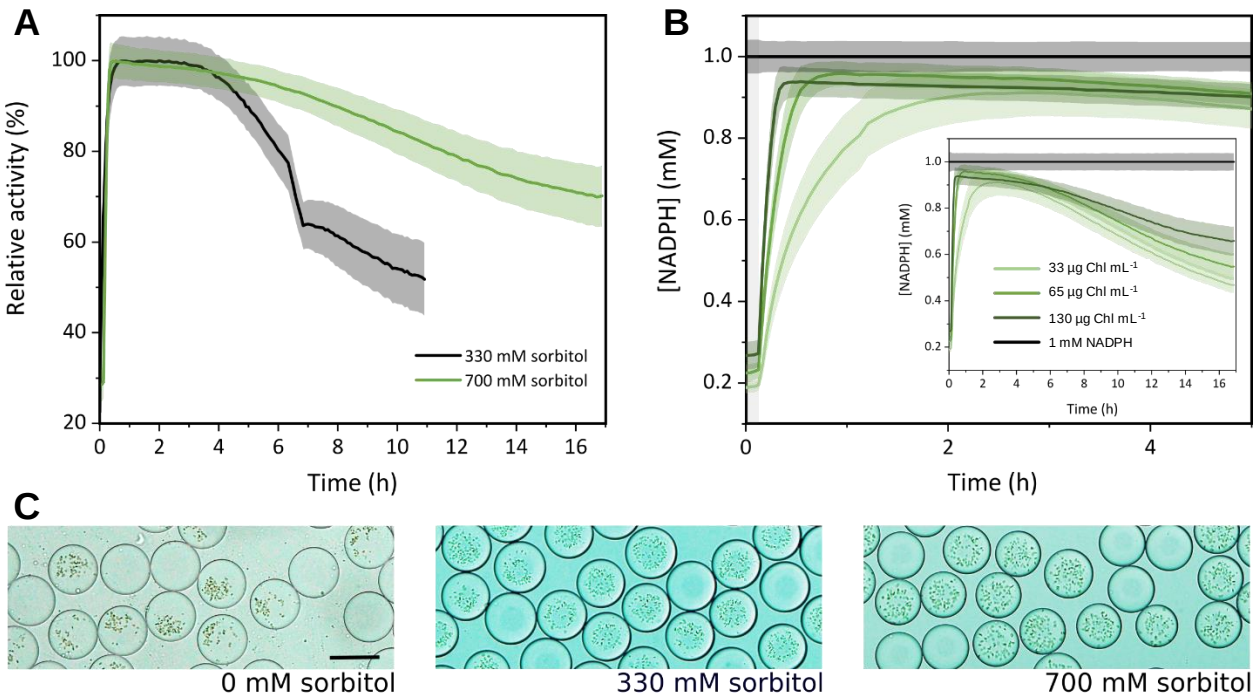

Fig. S11. TEM stability in droplets.

(**A**) Relative thylakoid activity ([NADPH]/[NADPH]$_{max}$) over time under continuous illumination (100 µmol photons m^{-2} s^{-1}) using either 330 mM or 700 mM sorbitol in the reaction buffer. The relative activity is defined as the NADPH concentration normalized to its maximum value. (**B**) NADPH produced from TEM. NADPH concentration over time under continuous illumination (100 µmol photons m^{-2} s^{-1}) using 700 mM sorbitol for either 130, 65, or 33 µg Chl mL^{-1}. NADPH concentration of all populations was corrected for the non-catalytic oxidation observed in the NADPH-only control. The average measurements are indicated by a bold line with corresponding error bars (± standard deviation; N = 50). (**C**) Droplets imaged after an overnight experiment (14-16 hours). The increasing sorbitol concentration prevents aggregation and improves the distribution of the TEM.

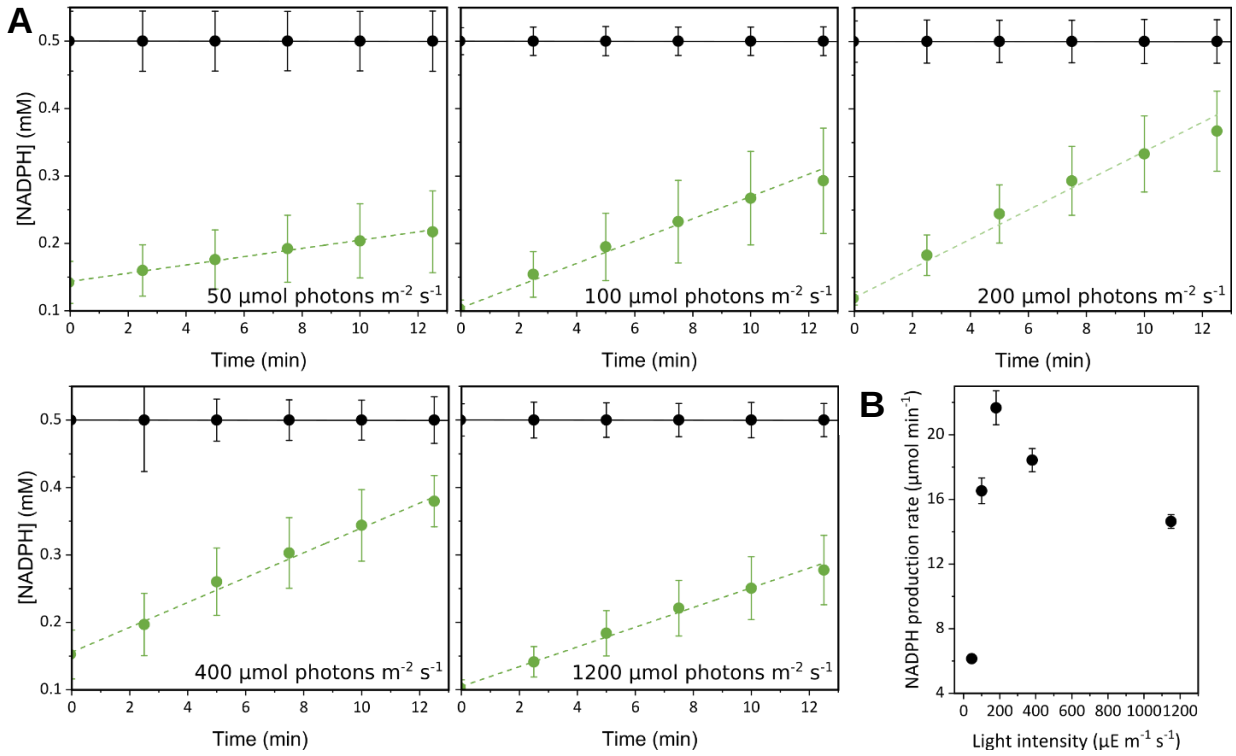

Fig. S12. Effect of light intensity on NADPH production of TEM encapsulated in droplets. (**A**) NADPH production rates (green points) of 130 µg Chl/mL TEM encapsulated in microdroplets under continuous illumination using 50, 100, 200, 400 or 1200 µmol photons m^{-2} s^{-1} and 0.5 mM $NADP^+$. Black lines show 0.5 mM NADPH in microdroplets lacking thylakoids. (**B**) NADPH production rate versus light intensity. Maximum NADPH production of around 200 µmol photons m^{-2} s^{-1} is achieved. However, we opted to operate the TEM at 50-60 µmol photons m^{-2} s^{-1} in order to limit the production of ROS that would damage the TEM. Depicted are the mean values with error bars that correspond to ± standard deviation (*N = 50*).

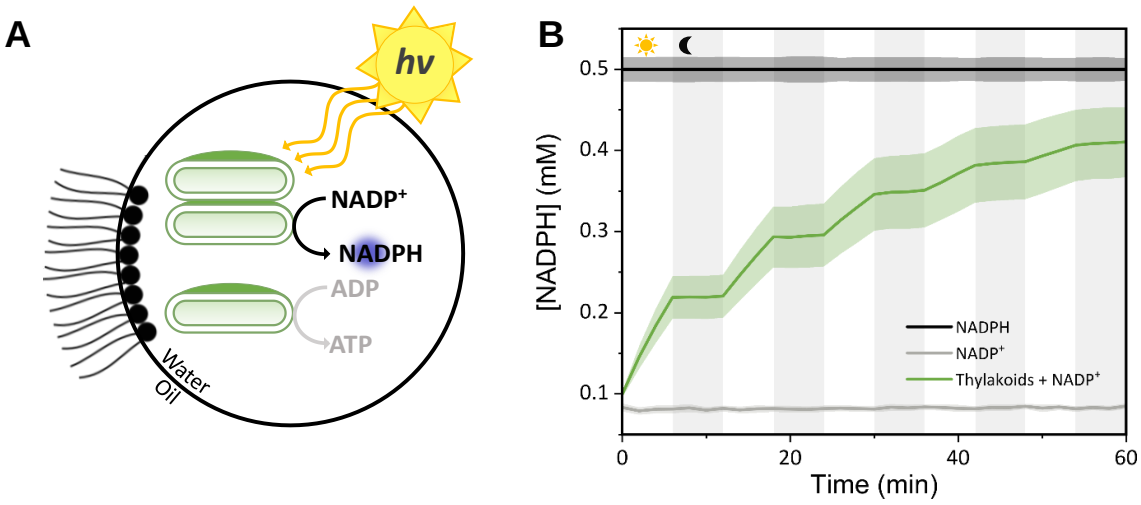

Fig. S13. Control of NADPH production by TEMs encapsulated in droplets through light-dark cycles.

(**A**) Scheme of the TEM system in microdroplets. Light triggers thylakoid activity to produce ATP and NADPH. NADPH production is monitored through fluorescence measurements. (**B**) NADPH concentration over time under programmed light-dark cycles (50 µmol photons m^{-2} s^{-1}/dark) using TEM (65 µg Chl mL^{-1}) and 0.5 mM $NADP^+$ (green line). NADPH production stops almost immediately when the light is turned off. Controls: 0.5 mM NADPH in droplets (black line), 0.5 mM $NADP^+$ in droplets (grey line) and TEM (65 µg Chl mL^{-1}) with 0.5 mM NADPH (green line). NADPH concentration of all populations was corrected for the non-catalytic oxidation observed in the NADPH-only control (0.5 mM NADPH in droplets, black line). This demonstrates that the energy status of the droplets can be controlled using light as an external signal. The average measurements are indicated by a bold line with corresponding shading indicating the standard deviation (*N = 50*).

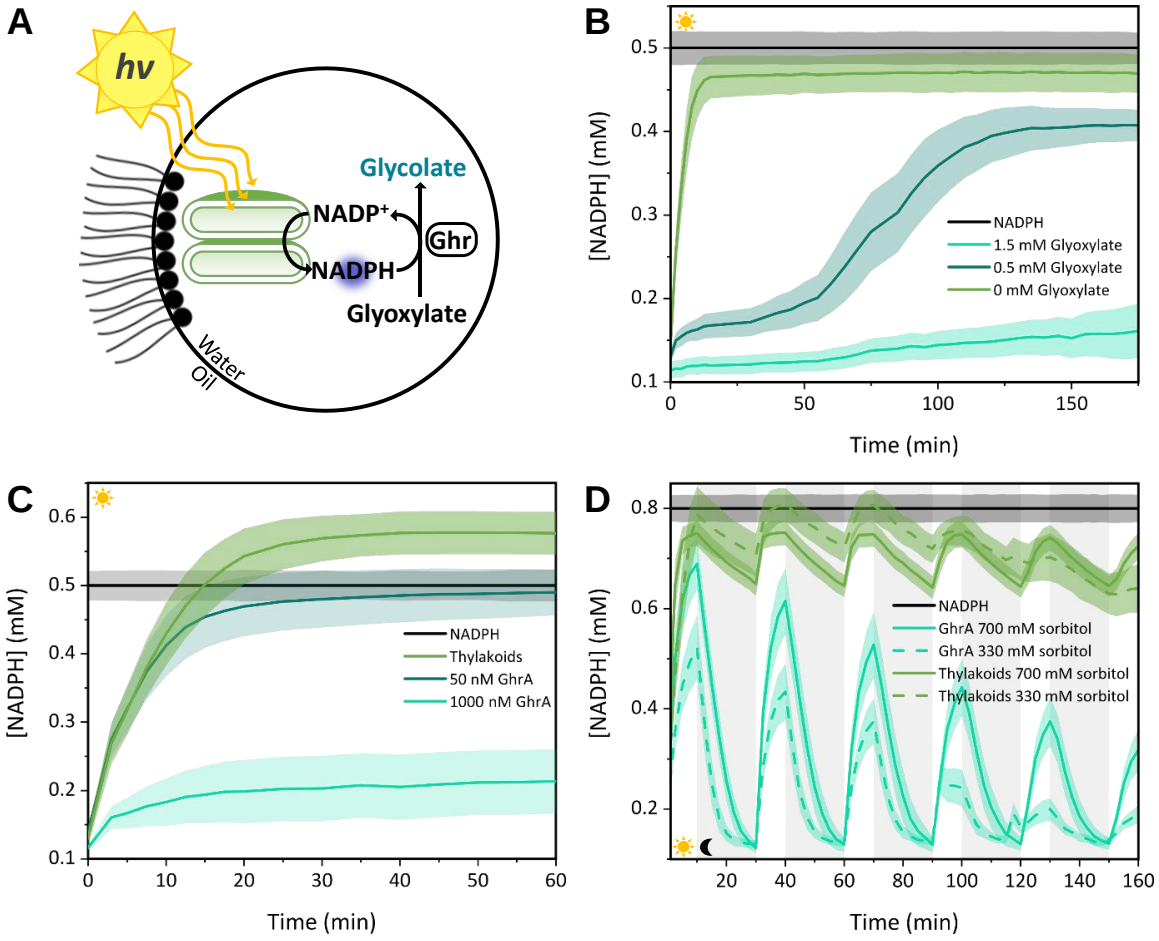

Fig. S14. Coupling the NADPH-dependent reduction of glyoxylate to TEMs in droplets demonstrates how metabolic activity and energy levels can be controlled in droplets externally.

By coupling the NADPH-dependent reduction of glyoxylate to the TEM in droplets we demonstrate the control that can be achieved in droplets by varying the internal content and externally regulating the droplet by illumination. (**A**) Scheme of the TEM/Ghr coupled system in microdroplets (as found in the main text). The light triggers TEM activity to produce NADPH, which is used by Ghr to catalyze the reduction of glyoxylate into glycolate. (**B**) NADPH concentration over time under continuous illumination (100 µmol photons m^{-2} s^{-1}) for different glyoxylate concentrations (0.5, 1.5 mM and 150 µg Chl mL^{-1}). As substrate is consumed, the NADPH level increases. (**C**) NADPH concentration over time under continuous illumination (50 µmol photons m^{-2} s^{-1}) for different concentrations of the enzyme Ghr, added at 0, 50, & 1000 nM with 65 µg Chl mL^{-1}. Different dynamic equilibrium states can be observed; as the concentration of Ghr increases, the maximum NADPH level reached decreases. Both (**B**) and (**C**) show how the internal composition can be modified to control the activity in the droplets. (**D**) TEM (120 µg Chl mL^{-1}) is coupled to Ghr (30 nM) and NADPH concentration is observed over time under fluctuating light conditions (50 µmol photons m^{-2} s^{-1} and dark). When the light is on, the TEM produces NADPH, and in the dark the oxidation of NADPH catalyzed by Ghr can be observed. This is a method for synchronizing the activity in droplets and could be useful in future kinetic studies in droplets. An increase of TEM stability is observed in droplets containing 700 mM sorbitol (solid line) in contrast to droplets

containing only 330 mM sorbitol (dashed line), where the TEM activity collapses after three light/dark cycles. NADPH concentration of all populations was corrected for the non-catalytic oxidation observed in the NADPH-only control.

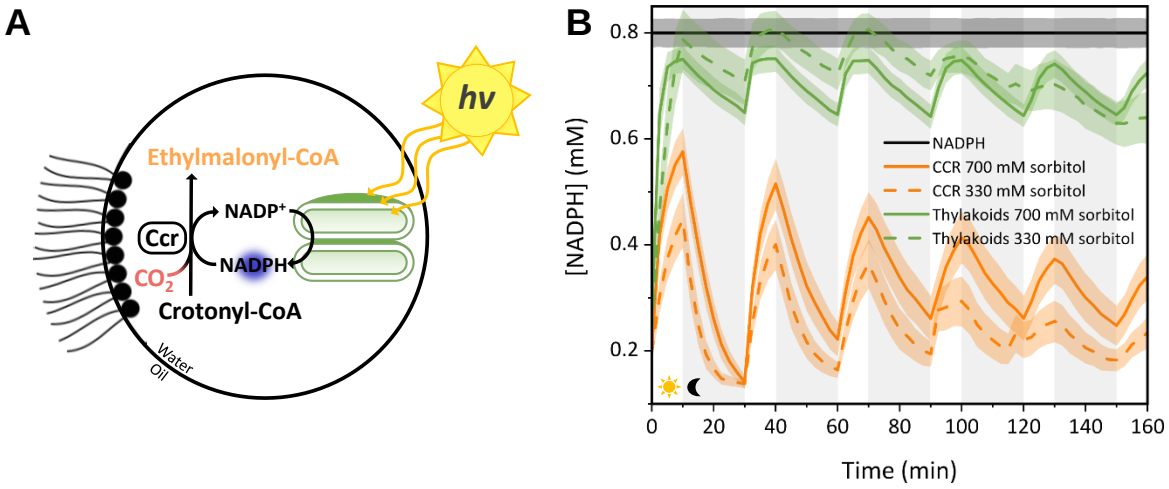

Fig. S15. Coupled single carboxylase reaction to TEM controlled with an external signal.
(**A**) Scheme of the TEM/Ccr-coupled system in microdroplets. Light triggers TEM-dependent production of NADPH, which is used by crotonyl-CoA carboxylase/reductase (Ccr) to catalyze the reductive carboxylation of crotonyl-CoA to ethylmalonyl-CoA. (**B**) NADPH concentration over time under light (50 µmol photons m^{-2} s^{-1}) and dark cycles of TEM (120 µg Chl mL^{-1}) coupled to Ccr (42 nM) in microdroplets. TEM in microdroplets is shown in green, Ccr coupled to TEM in microdroplets is shown in orange. Similar to the Ghr coupling experiment seen in fig. S14D, a stabilizing effect of increased sorbitol can be observed (solid lines represent droplets containing 700 mM sorbitol and dashed lines 330 mM). NADPH concentration of all populations was corrected for the non-catalytic oxidation observed in the NADPH-only control (0.8 mM NADPH).

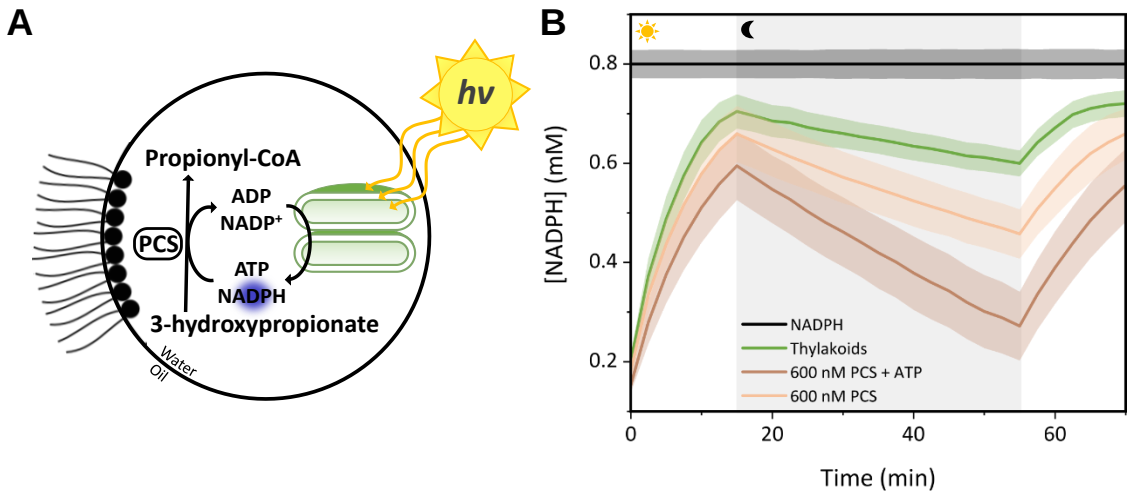

Fig. S16. Propionyl-CoA Synthase coupled to TEM

(**A**) Scheme of the TEM/Pcs-coupled system in microdroplets. Light triggers TEM activity to produce NADPH and ATP, which are used by propionyl-CoA synthase (Pcs) to catalyze the synthesis of propionyl-CoA from 3-hydroxypropionate. (**B**) NADPH concentration over time under fluctuating light (50 µmol photons m^{-2} s^{-1})-dark cycles of the TEM (82 µg Chl mL^{-1}) coupled to the Pcs reaction (with 100 nM Pcs, 5 mM CoA, 5 mM 3-hydroxypropionate, 0.8 mM $NADP^+$, and 1.2 mM ATP or ADP). TEM in microdroplets is shown in green, Pcs coupled to TEM in microdroplets is shown in orange, Pcs coupled to TEM and additional ATP in micro-droplets is shown in brown. In droplets that contain additional ATP, more NADPH oxidation can be observed, indicating that ATP production (or ADP inhibition) is limiting the Pcs reaction. NADPH concentration of all populations was corrected for the non-catalytic oxidation observed in the NADPH-only control (black line).

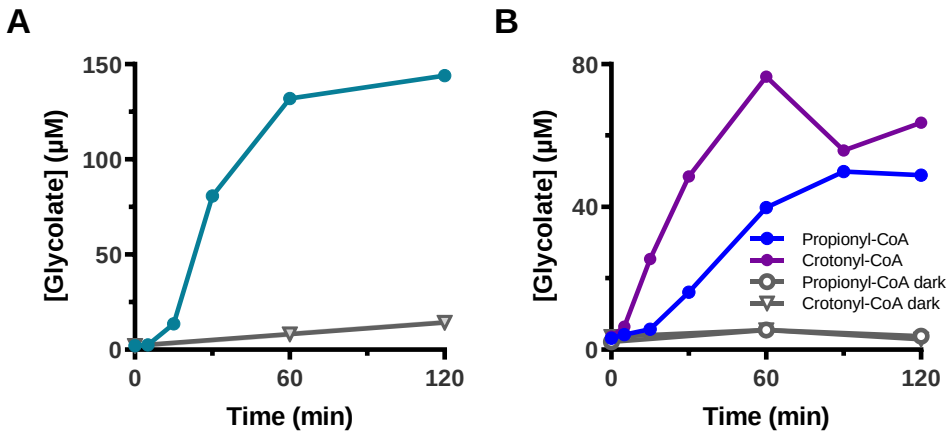

Fig. S17. Optimizing preparation of microdroplets for operating the CETCH cycle with TEM.

During encapsulation, the reaction mixture incubates for about one hour in the dark and at room temperature. To assess the effect of prolonged incubations of the reaction mixture before illumination, we measured glycolate production rates of CETCH v7.0 coupled to TEM in bulk with simulated conditions during encapsulation. (**A**) Glycolate formed starting from 120 µM propionyl-CoA when reactions are illuminated directly after mixing (teal line) or kept in dark conditions (grey line). (**B**) Glycolate formed when starting from both propionyl-CoA (blue) and crotonyl-CoA (purple) (120 and 90 µM, respectively) after one hour incubation in the dark. Samples were taken at 0, 5, 15, 30, 60, 90, and 120 minutes after illumination (60 µmol photons m^{-2} s^{-1}) or at 0, 60, and 120 minutes after the initial 1-hour incubation for samples that remained in the dark. These results from a representative experiment suggest that, with prolonged incubation times, starting from crotonyl-CoA leads to higher production rates compared to starting from propionyl-CoA. This might be explained by adenylate kinase activity producing ATP in the dark (see fig. S1C), which allows propionyl-CoA carboxylase (Pcc) to carboxylate propionyl-CoA to methylmalonyl-CoA, which is subsequently converted into succinyl-CoA. Succinyl-CoA is prone to spontaneous hydrolysis, likely lowering overall productivity of the system. As a result, we used crotonyl-CoA, and not propionyl-CoA as described by Schwander et al. *(23)*, to prepare CETCH- and TEM-containing microdroplets, mimicking the chloroplast.

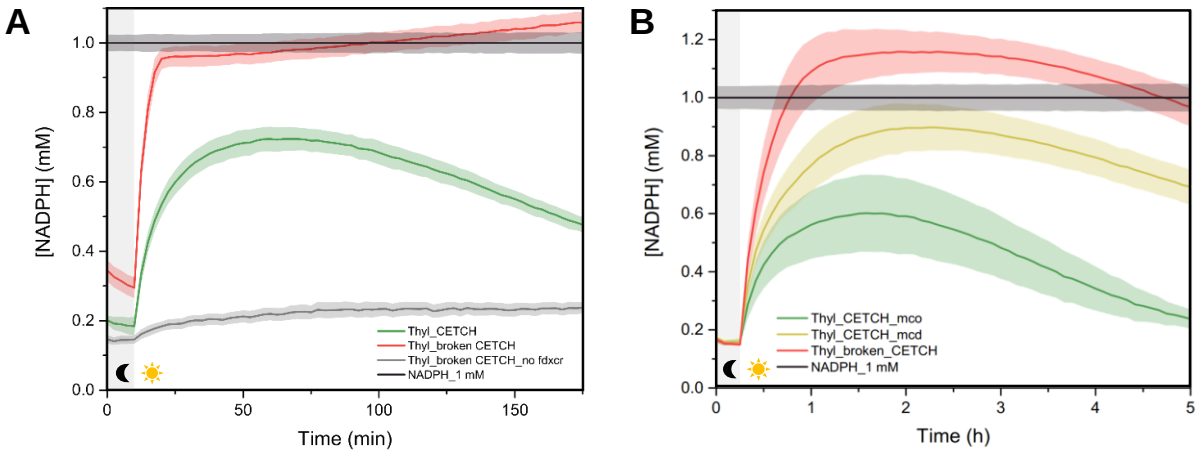

Fig. S18. Dynamic equilibrium monitoring of various versions of the CETCH cycle powered by TEM.

(**A**) Different versions of CETCH v6.0 coupled to TEM (70 µg Chl mL^{-1}) in microdroplets. Droplets containing a functional TEM, 1 mM $NADP^+$ and a functional CETCH v6.0 (with Mco, green line), as well as control droplets containing TEM, 1 mM $NADP^+$ and all enzymes of CETCH v6.0 except Ccr (red line), droplets containing TEM, 1 mM $NADP^+$, all enzymes of CETCH v6.0 except Ccr and no ferredoxin (grey line), as well as control droplets containing 1 mM NADPH. The dynamic equilibrium level of NADPH (indicating TEM activity) decreases after 100 minutes in droplets containing a functional CETCH v6.0 cycle. (**B**) Comparison of CETCH v6.0 (with Mco, green line) as shown in (**a**) and CETCH v7.0 (with Mcd, yellow line). Droplets with CETCH v7.0 maintain the dynamic equilibrium level of NADPH longer than droplets with CETCH v6.0, which is likely due to the use of Mcd instead of Mco.

Table S1.

Carbon fixation and ATP and NADPH regeneration rates of natural and synthetic systems compared to rates achieved in this study (normalized per mg chlorophyll).

Listed are CO_2-fixation, ATP and NADPH generation rates of isolated chloroplasts and thylakoids, other synthetic systems and the system of this study. For single-enzyme CO_2-fixing reactions (Ccr and Pcc), our integrated system is capable of fixing CO_2 at 124 µmoles mg Chl^{-1} h^{-1}, which is within the range of natural systems (38-280 µmoles mg Chl^{-1} h^{-1}). In bulk experiments with isolated thylakoids, NADPH and ATP regeneration rates are better than previously reported, yet lower than those measured with intact chloroplasts. In droplets, the regeneration of NADPH is of similar magnitude. Note that these rates are dependent on light intensity and could be improved by using higher light intensities. Furthermore, for the CETCH cycle operation, TEM is added in amounts so that cofactor regeneration is not limiting. Limiting the TEM would improve the rates on a per chlorophyll basis.

		Reported rates (µmoles/mg Chl/hour)		**Calculated or measured rates (µmoles/mg Chl/hour)**		
	Measurement	Carbon fixation rate	O_2 evolution	ATP	NADPH	Source
Natural	Isolated chloroplasts	50	--	--	--	Kalberer, et al. 1967 (*47*)
	Isolated chloroplasts	130-280	--	--	--	Heber et al. 1978 (*48*)
	Isolated chloroplasts	40-60	--	--	--	Reeves and Hall 1973 (*49*)
	Isolated chloroplasts (Spinach)	38	--	--	--	Avron and Gibbs, 1974 (*50*)
	Isolated chloroplasts	--	55	165*	110*	Heber, 1973 (*51*)
	Isolated chloroplasts	--	122	367*	245*	Heineke et al., 1989 (*52*)
	Isolated chloroplasts	--	231	693*	462*	Stitt, 1986 (*53*)
	Isolated thylakoid membranes *(in vitro)*	--	--	--	27 ± 3	Yacoby et al., 2011 (*54*)
Synthetic	Reconstituted photosynthetic system			0.9	--	Feng et al., 2015 (*19*)
This work	ATP & NADPH measurements bulk	--	71.5‡	65	143	This work (Fig. 1A, B, and fig. S1B)
	TEM in droplets	--	11.8‡	--	23.5	This work (Fig 3C)

	Ccr in droplets	6.4†	--	--	--	This work (measured values, Ccr 1-bit experiment)
	Pcc and Ccr reaction in bulk	124	30.5‡	62**	61**	This work (Fig. 1D)
	CETCH in bulk	0.55†	>2.2‡‡	--	--	This work (Fig. 2D)
	CETCH in Droplets	0.21†	>0.84‡‡	--	--	This work (CETCH v7.0 in droplets)
	ATP & NADPH measurements bulk	--	71.5‡	65	143	This work (Fig. 1A, B, and fig. S1B)

* Calculated from the O_2 evolution assuming for every 1 O_2 generated there are 2 NADPH and 3 ATP produced

** From the carbon fixation rates in bulk of single carboxylation reactions

† TEM was added in excess. On a per Chl or PSII basis, we expect higher rates when thylakoids are limiting.

‡ Calculated with the NADPH production or from the NADPH dependent reaction, assuming a 2:1 ratio NADPH:O_2

‡‡ Calculated with NADPH dependent reactions, 4 NADPH consumed per glycolate formed, assuming a 2:1 ratio NADPH:O_2

Table S2.

Comparison of carbon fixation and ATP regeneration rates of natural and synthetic systems compared to rates achieved in this study normalized to the chromophore.

Reported CO_2-fixation rates of natural and synthetic systems compared to rates achieved in this study. As above, rates of TEM-powered single CO_2 fixation reactions (68,600 molecules $PSII^{-1}$ h^{-1}) are comparable to rates in natural systems (21,100-155,500 molecules $PSII^{-1}$ h^{-1}). Compared to other synthetic systems, we achieve 2 to 3 orders of magnitude higher ATP generation rates and single CO_2-fixation reactions. For all calculations, 617 chlorophylls per PS II were assumed (*55*), except for the system described by Lee et al. that was calculated using 35 chromophores per PS II (*18*).

		Molecules / PSII reaction center / hour			
Natural	Isolated chloroplasts	27,800	--		Kalberer, et al. 1967 (*47*)
	Isolated chloroplasts	72,200-155,500	--		Heber et. al. 1978 (*48*)
	Isolated chloroplasts	22,200-33,300	--		Reeves and Hall, 1973 (*49*)
	Isolated chloroplasts (Spinach)	21,100	--		Avron and Gibbs 1974 (*50*)
Synthetic or Hybrid	CO_2 Fixation-single reaction	34*			Lee et al., 2018 (*18*)
	ATP production		29*		Lee et al., 2018 (*18*)
	ATP Production		500		Feng et al., 2015 (*19*)
	O_2 evolution			9000	Sokol et al., 2018 (*5*)
This work	ATP production		36000		This work (Fig. 1B)
	Ccr in droplets	3600†			This work (measured values, Ccr 1-bit experiment)
	Ghr in droplets	21300† **			This work (measured values, Ghr 1-bit experiment)
	O_2 evolution			26600	This work (fig. S2E, calculated from first 2 minutes)
	Pcc and Ccr reaction in bulk	68600			This work (Fig. 2D, CETCH v6.0 in bulk)
	CETCH in bulk	303†			This work (CETCH v7.0 in droplets)
	CETCH in Droplets	119†			This work (measured values)

* Calculated using 35 chromophore per PSII (*18*)

** Reaction rate, not a carbon fixation rate.

† TEM was added in excess. On a per Chl or PSII basis, we expect higher rates when thylakoids are limiting.

Table S3.

Enzyme concentrations used in CETCH experiments.

CETCH Cycle v6.0 and 7.0 enzyme composition

Enzyme full name	Organism	Name	Enzyme abbreviation	Concentration added (nM)
propionyl-CoA carboxylase	*M. extorquens*	PccAB	Pcc	*2310*
emC/mmC epimerase	*R. sphaeroides*	Epi	Epi	*20*
methylmalonyl-CoA mutase	*R. sphaeroides*	Mcm	Mcm	*360*
succinyl-CoA reductase	*C. kluyveri*	SucD	Scr	*194*
succinic semialdehyde reductase	*H. sapiens*	AKR7a2	Ssr	*670*
4-hydroxybutyryl-CoA synthetase	*N. maritimus*	Nmar0206	Hbs	*5890*
4-hydroxybutyryl-CoA dehydratase	*N. maritimus*	Nmar0207	Hbd	*560*
crotonyl-CoA carboxylase/reductase	*M. extorquens*	Ccr	Ccr	*580*
ethylmalonyl-CoA mutase	*R. sphaeroides*	Ecm	Ecm	*550*
methylsuccinyl-CoA oxidase	*R. sphaeroides.*	Mco	Mco	*21410*
methylsuccinyl-CoA dehydrogenase	*R. sphaeroides*	Mcd	Mcd	*3000*
electron transport flavoprotein	*R. sphaeroides*	Etf A/B	Etf	*1000*
Etf ubiquinone oxidoreductase	*P. migulae*	Etf:QO	Etf:QO	*8000*
mesaconyl-CoA hydratase	*R. sphaeroides*	Mch	Mch	*30*
β-methylmalyl-CoA lyase	*R. sphaeroides*	Mcl1	Mcl1	*2720*
glyoxylate reductase	*E. coli*	GhrA	Ghr	*1300*
enoyl-CoA hydratase	*P. aeruginosa*	PhaJ	PhaJ	*14000*

The enzyme highlighted in blue is Mco that was used in CETCH v6.0, and those highlighted in orange are those used in CETCH v7.0. The last two enzymes, highlighted in green, are used in the cycle but are not part of the core reactions.

Table S4.

Detailed pipetting schemes of multiplexed Ghr coupling experiments. Some internal components were varied (either enzyme concentration or substrate concentration). In each experiment, four populations were multiplexed and analyzed simultaneously. Grey boxes indicate the component was omitted, and concentrations of components that were varied are indicated.

		Protein concentration				**Substrate concentration**			
		Droplet population				Droplet population			
Component	Concentration	1	2	3	4	1	2	3	4
HEPES·KOH, pH 7.8	100 mM								
Sorbitol	330 mM								
K_2HPO_4	3 mM								
KCl	10 mM								
$MgCl_2$	5 mM								
Sodium L-ascorbate	10 mM								
Catalase	0.1 mg/mL								
Ferredoxin	5 µM								
Superoxide Dismutase	52 U/mL								
ADP	0.75 mM								
$NADP^+$	0.5 mM				-				-
NADPH	0.5 mM	-	-	-		-	-	-	
Glyoxylate	mM	-	0.5	0.5	-	-	0.5	1.5	-
GhrA	nM	50	50	1000	50	1000	1000	1000	1000
Thylakoids	µg mL^{-1}	65	65	65	-	150	150	150	-
Sulforhodamine B	µM	2	8	20	40	2	8	20	40

Table S5.

Detailed pipetting schemes of single enzyme coupling experiments. Ccr and Ghr were coupled in parallel two times either with 700 or 330 mM sorbitol. Grey boxes indicate the component was omitted, and concentrations of components that were varied are indicated.

330 or 700mM Sorbitol Ccr and GhrB Coupling

		Droplet population			
Component	Concentration	1	2	3	4
HEPES·KOH	100 mM				
Sorbitol	700 or 330 mM				
K_2HPO_4	5 mM				
KCl	10 mM				
$MgCl_2$	5 mM				
Sodium L-Ascorbate	10 mM				
Catalase	0.1 mg mL^{-1}				
Ferredoxin	5 µM				
Superoxide Dismutase	52 U mL^{-1}				
Ccr	41.8 nM				
GhrB	53.5 nM				
Carbonic anhydrase	33.5 nM				
Crotonyl-CoA	5.0 mM				
Glyoxylate	5.0 mM				
$NaHCO_3$	50 mM				
ADP	1.6 mM				
$NADP^+$	0.8 mM				
NADPH	0.8 mM				
Thylakoids	120 µg Chl mL^{-1}				
Sulforhodamine B	µM	2	8	16	40

Table S6.

Detailed pipetting schemes of Pcs coupling experiments. Grey boxes indicate the component was omitted, and concentrations of components that were varied are indicated.

Pcs Coupling

		Droplet population			
Component	Concentration	1	2	3	4
HEPES·KOH, pH 7.8	50 mM				
Sorbitol	330 mM				
K_2HPO_4	3 mM				
KCl	10 mM				
$MgCl_2$	5 mM				
Sodium L-Ascorbate	10 mM				
Catalase	0.1 mg mL^{-1}				
Ferredoxin	5 µM				
Superoxide Dismutase	52 U mL^{-1}				
Pcs	100 nM				
CoA	5 mM				
3-Hydroxypropionate	5 mM				
ADP	1.2 mM				
ATP	1.2 mM				
$NADP^+$	0.8 mM				
NADPH	0.8 mM				
Thylakoids	80 µg Chl mL^{-1}				
Sulforhodamine B	µM	2	4	20	40

Table S7.

Detailed pipetting schemes of individual multiplexed CETCH experiments. Grey boxes indicate the component was omitted, and concentrations of components that were varied are indicated.

		Fig. S18 A				Fig. S18 B				Fig. 4 B-C			
		Droplet population				Droplet population				Droplet population			
Component	Concentration	1	2	3	4	1	2	3	4	1	2	3	4
HEPES·KOH, pH 7.8	100 mM												
Sorbitol	700 mM												
K_2HPO_4	5 mM												
KCl	10 mM												
$MgCl_2$	5 mM												
Sodium L-Ascorbate	10 mM												
Catalase	1.2 µM												
Ferredoxin	5 µM												
Superoxide Dismutase	52 U/mL												
mcd	3 µM												
etf	8 µM												
etf:QO	1 µM												
mco	21.4 µM												
Ccr	580 nM												
Other CETCH core enzymes, see Table S3													
Ppk	1.6 µM												
polyphosphate	10 mM												
Carbonic anhydrase	33.5 nM												
Crotonyl-CoA	250 µM												
phaJ	14 µM												
GhrA	1.3 µM												
$NaHCO_3$	50.0 mM												
CoA	0.5 mM												
ADP	mM	1.6	1.6	1.6	1.6	1.6	1.6	1.6	1.6	1.2	1.2	1.2	1.2
$NADP^+$	0.8 mM												
NADPH	0.8 mM												
Thylakoids	µg Chl mL^{-1}	70	70	70		70	70	70		60	60	60	
Sulforhodamine B	µM	2	8	16	40	2	8	16	40	2	8	16	40

Table S8.

List of vectors used in this work.

Vector	Relevant features	Source or reference
pET28a-PPK	pET28a, SMc02148 (codon optimized Ppk2), kan^r	Nocek et al., 2008 PNAS (*56*)
Nmar0206	pET16b, nmar0206, amp^r	Könneke et al. 2014, PNAS (*57*)
p2BP1	pLIC-SGC1, akr7a2, amp^r	Addgene plasmid #39130
pBB541	*E. coli* Chaperones GroEL, GroES, $spectinomycin^r$	Addgene plasmid #27394
pRKisc	*E. coli* ORF2-iscS-iscU-iscA-hscB-hscA-fdx-0RF3 Gene Cluster Involved in the Assembly of Fe-S Clusters, tet^r	Nakamura et al. 1999, J. Biochemistry (*41*)
pMCH_RS_JZ06	pET16b, mch, amp^r	Zarzycki et al. 2008, J. Bacteriol (*58*)
pMCL1_RS_JZ03	pET16b, mcl1, amp^r	Erb et al. 2010 J. Bacteriol. (*59*)
JW5656	pCA24N,tiaE, cam^r, ASKA collection	Kitagawa et al. 2005, DNA Res (*60*)
JW5146	pCA24N, ycdW, cam^r, ASKA collection	Kitagawa et al. 2005, DNA Res (*60*)
JW1721	pCA24N, katE, cam^r, ASKA collection	Kitagawa et al. 2005, DNA Res (*60*)
pET21a(+)-fdh_{D221A}	pET21, fdh (D221A), amp^r	Hoelsch et al. 2013, Appl. Microbiol. Biotechnol. (*61*)
pTE22	pET16b, mcd, amp^r	Erb et al. 2009, Mol. Microbiol. (*62*)
pTE33A	pET16b, ecm, amp^r	Erb et al. 2008, JBC. (*63*)
pTE45	pET16b, epi, amp^r	Erb et al. 2008, JBC. (*63*)
pTE46	pET16b, mcm, amp^r	Schwander et al. 2016, Science (23)
pTE71	pET16b, ccr, amp^r	Rosenthal et al. 2014 Nat. Chem. Biol. (*64*)
pTE1012	pSEVA 471, Propionyl-CoA synthetase (Erythrobacter sp. Nap-1) optimized for E. Coli	Bernhardsgrütter et al. 2019, JACS (*37*)
pTE701	pET28a, His-phaJ from *P. aeruginosa* (codon optimized), kan^r	Schwander et al. 2016, Science (*23*)
pTE2101	pET28a, ETF:QO from *P. migulae*, codon optomized, kan^r	this work, BaseClear
pTE380	pCDFDuet-1, 6xHis-sucD, yihU, $streptomycin^r$	Schwander et al. 2016, Science (*23*)
pTE392	pCDFDuet-1, His-etfA, etfB, *R. sphaeroides*, $streptomycin^r$	Schwander et al. 2016, Science (*23*)
pTE393	pRSET B, nmar0207 (codon optimized), amp^r	Schwander et al. 2016, Science (*23*)
pTE801	pET16b, mcd, amp^r	Schwander et al. 2016, Science (*23*)
pTE826	pTE16b, "pco" acx4_opt (T134I), amp^r	Schwander et al. 2016, Science (*23*)
pTE813	pET16b, "mco" mcd (T317G, W315F, E377N), amp^r	Schwander et al. 2016, Science (*23*)
pASK-IBA7-FNRCr	pASK-IBA7, n-term strep tag, FNR *C. reinhardtii*, transit peptide removed, amp^r	Rumpel et al., 2014, Energy & Environmental Science (*36*)
pTE2001	pEX-A2-Fdx, petF *C. reinhardtii* (codon optimized), transit peptide removed, amp^r	Eurofins MWG
pTE2002	pET16b, petF *C. reinhardtii* (codon optimized), transit peptide removed, n-term strep tag, amp^r	This work
pTE2003	pEX-A2-3_Fdx, Fdx1 *S. oleracea* , Fdx2 spinach, Fdx2 *A. thaliana*, codon optimized, transit peptides removed, amp^r	Eurofins MWG

pTE2004	pET16b, fdx1 Spinach (codon optimized), transit peptide removed, n-term strep tag, amp^r	This work
pTE2005	pET16b, petF Spinach (codon optimized), transit peptide removed, n-term strep tag, ampr	This work
pTE2006	pEX-A2_FNRSp, FNR Spinach (codon optimized), transit peptide removed, n-term strep tag, amp^r	Eurofins MWG
pTE2007	pASK-IBA7, n-term strep tag, FNR spinach (codon optimized), transit peptide removed, amp^r	This work
pTE2008	pET16b, ETF:QO from *R. sphaeroides 2.4.1*, amp^r	This work

Table S9.

DNA sequence of the codon optimized genes used in this work

Gene name	Codon optimized DNA sequence
FdxCr (petF) from *C. reinhardtii*	TACAAGGTCACCCTGAAAACCCCTAGCGGCGATAAAACGATTGAGTGCCCAGCCGACACTTACATTTTG GATGCTGCTGAAGAGGCGGGGCTGGACCTGCCGTATTCGTGTCGCGCGGGTGCCTGCTCTTCATGCGCG GGCAAAGTGGCCGCAGGCACCGTGGATCAAAGCGACCAGTCATTCTTAGACGATGCGCAGATGGGTAA CGGTTTTGTGCTGACGTGTGTAGCTTATCCGACGAGTGATTGCACTATCCAAACACATCAGGAAGAAGC GCTGTATTAA
FdxSp1 (Fdx1) from *S. oleracea*	GCAGCATATAAAGTGACGCTGGTGACTCCGACCGGTAACGTAGAATTTCAGTGTCCTGATGACGTCTAT ATCCTTGATGCTGCTGAAGAGGAAGGCATCGATTTACCATACTCCTGTCGCGCCGGTTCGTGCTCAAGCT GCGCCGGTAAACTGAAGACGGGATCATTGAACCAAGACGATCAGAGCTTCCTGGACGACGACCAGATT GATGAAGGGTGGGTTCTGACATGCGCGGCGTACCCGGTGAGCGATGTTACCATTGAGACCCATAAGGAA GAAGAACTCACCGCGTAA
FdxSp2 (petF) from *S. oleracea*	GCGACTTACAAAGTCACCTTAGTTACACCATCTGGTTCACAAGTTATTGAATGTGGTGACGATGAATATA TCTTGGACGCCGCGGAAGAGAAAGGTATGGATCTGCCGTACTCCTGTCGCGCGGGCGCATGCTCGTCGT GCGCAGGTAAAGTAACTTCAGGCTCGGTGGACCAGAGCGATCAGAGCTTTTTGGAAGATGGACAGATG GAAGAAGGCTGGGTGCTCACATGCATAGCCTATCCGACCGGCGATGTGACGATCGAAACCCATAAGGA GGAAGAGTTGACCGCCTAA
FNRSp (FNR) from *S. oleracea*	ATGGCTAGCTGGAGTCATCCGCAATTTGAGAAAATCGAAGGTCGCCAGATTGCATCTGATGTGGAAGCC CCACCACCCGCTCCGGCGAAAGTGGAGAAACATAGCAAAAAAATGGAAGAAGGCATCACAGTTAATAA ATTTAAACCAAAAACACCTTATGTTGGACGATGCTTGTTGAATACCAAGATCACCGGCGATGACGCCCC TGGTGAGACTTGGCACATGGTCTTCTCCCACGAAGGCGAGATCCCTTACCGTGAGGGCCAATCGGTTGG GGTCATTCCGGATGGCGAAGATAAAAATGGTAAACCGCACAAACTGAGGCTGTACTCAATAGCCAGTA GCGCATTAGGGGATTTCGGGGATGCAAAGTCCGTCTCACTGTGCGTTAAACGCCTGATTTATACTAATGA CGCTGGTGAAACCATCAAAGGCGTATGCTCGAATTTTTTATGTGATCTGAAACCGGGCGCAGAGGTAAA GTTAACGGGCCCGGTGGGTAAAGAAATGCTGATGCCGAAGGACCCCAACGCAACCATTATTATGCTCGG TACTGGGACGGGCATTGCTCCGTTTCGTTCTTTTCTTTGGAAAATGTTTTTTGAGAAACACGATGATTATA AATTCAACGGTCTCGCCTGGCTATTCCTCGGTGTCCCGACGTCCTCATCGCTGCTGTACAAGGAAGAGTT CGAGAAAATGAAGGAAAAAGCTCCGGACAACTTCCGCCTTGATTTCGCGGTGAGCCGTGAGCAGACCA ACGAAAAAGGCGAAAAAATGTATATCCAGACCCGGATGGCGCAGTACGCGGTGGAACTGTGGGAAATG TTGAAAAAGGACAACACCTATTTTTATATGTGTGGTCTGAAAGGGATGGAGAAGGGCATTGATGACATT ATGGTGAGTCTTGCCGCGGCGGAAGGAATTGACTGGATCGAATACAAGCGCCAGCTGAAAAAAGCGGA ACAGTGGAACGTGGAAGTGTATTGA
ETF:QO$_{pm}$ (Etf:QO) from *P. migulea*	ATGGAGCGTGAGTACATGGAATTTGATGTCGTAATTGTTGGGGCTGGTCCTGCTGGTCTTTCTGCGGCGT GTCGCTTAAAGCAAAAAGCCGCAGAGGCTGGGAAAGAAATCAGCGTATGTGTTGTTGAAAAGGGGAGT GAGGTGGGTGCTCATATCTTATCTGGTGCTGTTTTTGAGCCACGCGCCCTGAATGAGCTGTTCCCTGACT GGAAGGAACTGGGAGCCCCTCTTAACACTCCTGTAACTCGCGATGATATCTTTGTGTTGAAAAATGCGG ATTCAGCACAAAAAATTCCAGACCTTTTTGTTCCAAAGACCATGCACAACGAGGGCAACTACATTATCT CCCTGGGAAATCTGTGTCGTTGGTTGGCCCAACAAGCAGAAAACTTAGGTGTAGAGATCTACCCGGGAT TTGCTGCGCAGGAGGCTCTGTTTGATGAAAATGGAGTAGTCCGTGGTATCATTACTGGGGATTTAGGTGT AGACCGTGAGGGACATCCCAAGGAGGGATTGTATACACCGGGTATGGAGTTACGTGGCAAGTATACGTT GTTCGCAGAAGGCTGCCGCGGTCATATTGGAAAACAATTGATTAAACGCTTCAACCTTGACTCGGAAGC TGATGCCCAACACTATGGTATTGGACTTAAAGAAATCTGGGAGATCGATCCAGCCAAACATCAGCCCGG GCTGGTCGTGCACACGGCGGGCTGGCCTTTAGACATCATGGGAACTGAGAACACAGGGGGTTCGTTTTT ATATCATCTTGAGAACAACCAGGTTGTCGTCGGTTTGATCGTTGACCTTTCATACTCCAACACGTATCTG TCCCCCTTTGATGAGTTTCAGCGTTTGAAGCATCACCCTGTTCTGAAGCAGTATCTGGAGGGTGGTAAAC GTATCTCGTATGGTGCACGCGCGATCTGCAAAGGCGGCCTGAACTCGCTGCCTAAAATGGTATTCAAGG GTGGTGCCCTTATCGGCTGCGATCTTGGAACTTTAAATTTCGCGAAGATCAAAGGATCACACACCGCCAT GAAGAGCGGGATGTTGGCGGCAGAAAGCGTGGCTGAGGCGCTTTTTGCGGAGAAGGATGGAACTGAGG AATTGACCACGTATGTCGATGCGTTTAAAAAATCGTGGCTTTATGACGAGTTGTTCGCCTCGCGTAATTT TGGGCCGGCTATTCACAAGTTCGGGGCCATTGTCGGTGGGGGCTTTAACTGGCTTGACCAGAATATCTTC GGAGGAAAACTTCCCTTCACGTTACACGACACTAAGCCCGACTACGCCTGCTTGAAACTTGCAGCGGAT TGTAAGAAAATCGATTATCCAAAGCCCGACGGTAAAATCTCTTTTGACAAACTGTCTAGCGTCTTTATTT CGGGTACGAATCACGAGGAAGAACAGCCTTGTCATCTGAAATTGACCGATCCCTCCATCCCCATCGCAA AAAATTTACCCATGTACGACGAACCTGCCCAGCGCTACTGTCCCGCGGGGGTTTACGAAGTCGTGACGA AGGAGGACGGGGAGAAACGTTTCCAAATCAATGCCCAGAACTGTGTTCATTGCAAAACGTGCGACATTA AGGATCCTGCTCAGAACATCACGTGGGTAGCGCCTGAAGGTGCTGGTGGCCCAACATACCCAAATATGT AA